Journal of Alloys and Compounds 818 (2020) 152918

Contents lists available at ScienceDirect

Journal of Alloys and Compounds

journal homepage: http://www.elsevier.com/locate/jalcom

Electromigration in Bi-crystal pure Sn solder joints: Elucidating the role of grain orientation

Marion Branch Kelly, Sridhar Niverty, Nikhilesh Chawla*

Center for 4D Materials Science, Interdisciplinary Science & Technology Building IV, Arizona State University, Tempe, AZ, 85287-6106, USA

ARTICLE INFO

Article history:
Received 12 August 2019
Received in revised form
16 October 2019
Accepted 4 November 2019
Available online 6 November 2019

Keywords:
Intermetallics
Semiconductors
Anisotropy
Diffusion
Crystal structure

ABSTRACT

Intermetallic compound (IMC) and void growth are electromigration (EM) damage mechanisms that are controlled by the anisotropic diffusion of Cu in β-tetragonal Sn solder joints. Single crystal fast diffusion, slow diffusion, and bicrystal solder joints were fabricated and tested under thermal aging and EM conditions to investigate the effect of grain orientation on microstructure evolution including IMC growth, void growth and grain structure. Sample and testing geometry ensured there were no effects from current crowding or joule heating so that crystallographic effects could be isolated. Microstructure characterization by scanning electron microscope (SEM), electron backscatter diffraction (EBSD) and X-ray microtomography revealed interface-nucleated and bulk-nucleated IMC growth, particle stimulated nucleation (PSN) of recrystallized grains, and two unique voiding behaviors, void faceting and void burrowing. The relationship between these features and β-Sn grain orientation and implications for EM damage mitigation are discussed.

1. Introduction

Electromigration (EM) is recognized as a critical reliability problem in microelectronic devices that will increase in severity as solder joints continue to decrease in volume [1,2]. Sn-rich alloys experience accelerated EM damage due to the β-tetragonal structure of the Sn matrix. Dyson and Turnbull first demonstrated the anisotropic interstitial diffusion of Cu in Sn in 1967 [3] and subsequent researchers showed that Sn also exhibits anisotropic elastic modulus, thermal expansion, and resistivity [4–6]. However, atomic diffusion is the most important parameter in EM of Pb-free solder joints because Cu interstitial diffusion results in the growth of the brittle IMCs Cu_6Sn_5 and Cu_3Sn and dissolution of under bump metallization (UMB) layers [7,8]. In addition, Sn self-diffusion creates a vacancy flux that opposes electron flow and causes void formation [1,2,6]. The fastest diffusion pathways are interstitial diffusion along the c-axis of β-Sn and grain boundary diffusion of Cu and Sn, meaning grain orientation and grain size are critical to the lifetime of a solder joint [3,9].

In the mid 2000's researchers began to focus on the effect of grain orientation and grain boundaries on EM damage. Lu and collaborators [10] demonstrated IMC buildup along grain boundaries parallel to the electron flow in bicrystal solder joints containing grains with very different c-axis orientations. Grains with the c-axis more closely aligned with the electron flow experienced rapid IMC growth due to Cu diffusion while grains with the c-axis perpendicular to the electron flow experienced void growth due to Sn diffusion along the grain boundary. The angle between the c-axis and electron flow was defined as the θ angle (also referred to as the α angle, but we will use θ for the sake of clarity). It was determined that a joint would be more resistant to EM when it contained grains with larger θ angles and more susceptible with smaller θ angles. Chen et al. [11] EM tested a series of polycrystalline solder joints with a range of θ angles and grain sizes. They correlated the average c-axis orientation of the joints with the thickness of the interfacial IMC that grew during testing. Samples with smaller θ angles had thicker interfacial IMC layers than those with larger θ angles [11]. Sn grain orientation relative to the electron flow clearly had a significant impact on IMC growth, however the grain structure of these joints was inconsistent. Each sample contained multiple grains with various orientations and grain sizes, complicating the relationship between grain orientation and IMC growth. Without pre-testing electron backscatter diffraction (EBSD) characterization it is also unclear if the grain structure was constant or evolved during testing, as we will show is possible. Grain boundaries are also rapid diffusion pathways for Cu and Sn, however the high

* Corresponding author.
E-mail address: nchawla@asu.edu (N. Chawla).

https://doi.org/10.1016/j.jallcom.2019.152918
0925-8388/

density of boundaries and variation between samples were not taken into account. In order to most accurately determine the effect of grain orientation on EM, specific c-axis orientations need to be isolated in single crystal joints instead of averaged over several grains. Tasooji, Lara, and Lee [12] investigated EM in a series of prefabricated C4 solder bumps and found that IMCs grew along high angle grain boundaries. They did not draw any clear relationships between grain orientation and IMC growth, likely due to the limited variation in orientation their bumps exhibited. In contrast Huang et al. [13] found grain orientation to be the controlling feature in IMC growth in their study on flip chip solder bumps, although IMC particles grew near grain boundaries instead of along them as reported by Lu et al. [10] and the samples contained different grain boundary densities. The discrepancies between these studies highlight the difficulty of interpreting EM results in polycrystalline samples. EM damage will be accelerated in Sn grains with low θ angles and samples with high grain boundary densities, but the relationships between microstructure and IMC morphology, distribution, and growth rate are still unclear. To focus on grain boundary and grain orientation effects, Huang et al. [14] conducted EM tests on solder joints with a single horizontal grain boundary between high and low θ angle grains. When electrons flowed from a low θ grain to a high θ grain, an IMC layer built up at the grain boundary. When electrons flowed from a high θ grain to a low θ grain, voids nucleated at the cathode Cu-solder interface and little IMC growth was observed. In this case, grain orientation determined whether voiding or IMC growth occurred rapidly, and the horizontal grain boundary affected where IMC particles would grow in the bulk. This result suggests that grain orientation determines whether a joint will fail due to crack propagation through interfacial voids or due to embrittlement caused by IMC growth. The presence of grain boundaries will affect where and how IMC particles coarsen, which in turn has been shown to affect the strength of the solder [7,15]. Further study of single and bicrystal solder joints will lead to greater understanding of the void and IMC growth that impact solder joint strength and reliability.

Most recently, Shen and Chen [16] discussed variations in interfacial IMC growth due to θ angles with the following conclusions: low θ angles result in rapid IMC growth, intermediate θ angles result in dissolution of interfacial IMC on the anode and regrowth on the cathode, and high θ angles result in no interfacial IMC growth. However, exclusively post-mortem analysis again makes the relationship between as-fabricated microstructure and IMC growth unclear and the variation in grain size makes individual bumps in this study difficult to compare. Tian et al. [17] expanded up this work in a 2018 study where they analyzed cross-sectioned polycrystalline SnCuNi solder joints before and after EM testing. They showed that when the c-axis of the Sn grain was aligned with the electron flow and directed towards the surface of the cross section, the growth of bulk IMC particles was visible as they formed hillocks that protruded from the sample surface. This study [17] and Huang et al.,'s 2015 [13] and 2016 [14] studies are some of the few to discuss growth of IMC particles in the solder bulk as opposed to grain boundaries and it is consistently correlated with low θ angle grains. Low θ angle β-Sn grains will experience slow Cu diffusion that builds up in the grain and causes IMC particles to nucleate in the solder bulk.

It is clear from this extensive body of work that both grain orientation and grain boundaries of β-Sn have a significant effect on EM damage. Research has shown that the θ angle of a Sn grain will affect IMC growth, both interfacial and bulk, as well as the rate of Cu dissolution and void growth. Grain boundaries appear to determine where IMC particles will nucleate or build up. However, determining consistent relationships between microstructure and EM damage has been complicated by the use of a variety of testing structures, from pre-fabricated solder bumps to solder bars or lines, which makes comparison between studies difficult as each testing geometry may result in different current crowding and joule heating effects [1,2]. The use of polycrystalline samples also limits the conclusions that can be drawn because grain boundary diffusion and grain orientation will always be confounded. The fabrication of multiple solder joints without current crowding and joule heating effects, with identical fabrication, and comparable grain orientations and grain sizes would simplify the investigation of grain orientation and boundary effects on EM damage. Furthermore, the majority of analysis is done on post-EM-tested sample cross sections which is effective at determining average changes in microstructure when compared to as-fabricated samples but cannot capture the initial state of a particular sample. Without a comprehensive understanding of the samples' initial state one cannot determine how its grain structure evolved into its final state, nor any relationship that the IMC or void growth may have had with the initial structure.

Finally, IMC growth and void growth are usually considered separately from one another and are only discussed as a direct result of orientation instead of in a dynamic relationship with it. This study will show how IMC growth, void growth, and grain structure evolution are interrelated processes that must be analyzed together to fully understand the microstructure that results from EM. Understanding these three processes in relation to each other will shed light on different IMC morphologies, Sn matrix recrystallization, and the phenomena of void faceting and burrowing. A simple and symmetric sample geometry ensures that there will be no localized current crowding or joule heating effects and a unique fabrication technique creates samples with comparable grain orientations and grain sizes. In order to fully capture the initial and final sample states SEM, EBSD, and X-ray microtomography analysis will be used in concert. SEM imaging will determine differences in surface characteristics such as hillock or IMC formation. Grain structure will be analyzed with EBSD to determine θ angles and microstructural changes due to testing or IMC growth. Most importantly, the initial and final 3D void and IMC morphologies will be quantified using nondestructive X-ray microtomography. This allows for the calculation of void and IMC growth rates and their relation to grain orientation, as well as 3D visualizations that are critical in understanding 2D SEM and EBSD analysis. This multimodal approach allows for the understanding of IMC growth, matrix transformation, and void evolution in a novel way.

2. Materials and experimental procedure

In order to isolate large single and bicrystal regions in the Sn solder, the solder joints were fabricated in a two-step process. First a larger initial sample was created and then it was sectioned into smaller solder bar joints, as seen in Fig. 1(a). The initial sample was a sandwich-style joint composed of a 250 μm thick Sn disc, cut from a Sn ribbon (Indium Corporation, 99.99% purity), placed between two oxygen-free high conductivity (OFHC) Cu pellets (McMaster-Carr, Cu alloy 101) with a diameter of 9.5 mm. The Sn ribbon was coated in Indalloy Flux #5 RMA (Indium Corporation) prior to stacking to remove Cu and Sn surface oxides during reflow. The completed solder stack was placed into a cylindrical metal tube with an inner diameter equal to the diameter of the Cu pellets. This confirmed that the pellets and Sn disc were aligned on top of one another. The stack was then compressed using a hand press to ensure even contact between the pellets and Sn disc. After pressing, the stack was removed from the tube for reflow. The solder stack was reflowed on a standard hot plate in ambient air with a hold of 20 s above 232 °C and then transferred to a pre-chilled Cu surface to

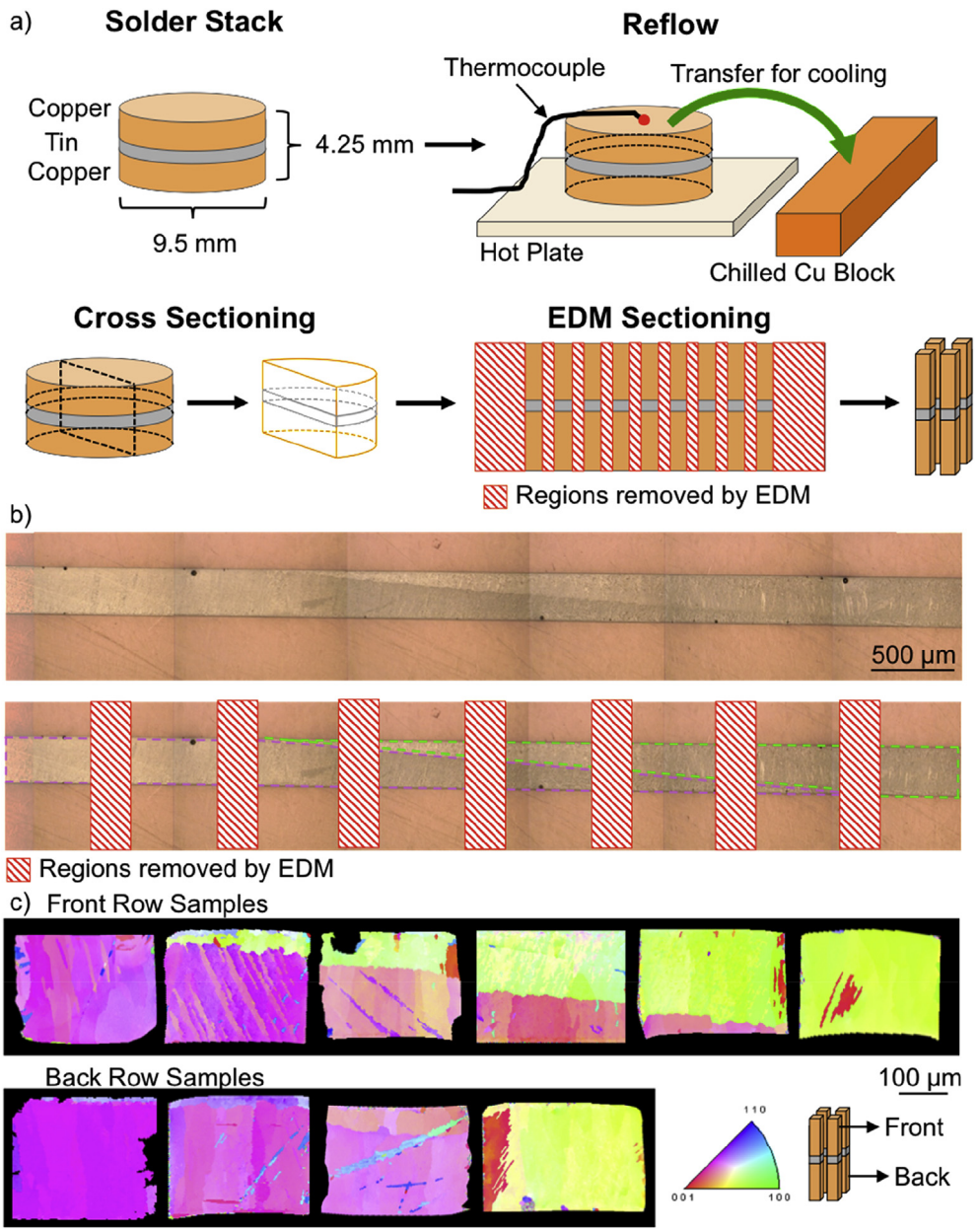

Figure 1. (a) Single and bicrystal solder bar fabrication procedure. (b) Polarized light microscope images of solder joint cross section, showing long slanted grain boundary. Green and pink dashed lines encompass the two predominant grains on either side of the boundary and expected regions of loss due to EDM sectioning are marked. (c) EBSD maps of the front surface of solder bars, showing multiple single crystal samples with pink and green grain orientations and a set bicrystal samples, created from the slanting grain boundary region indicated in (b).

cool at a rate of 3.4 °C/s. The solder stack was then cross-sectioned, mounted in epoxy, and mechanically polished finishing to a 0.05 µm colloidal silica finish. The thickness of the Sn region of the solder joint was 285 ± 2 µm. The final thickness was greater than the original thickness of the ribbon due to the molten Sn wicking between the Cu pellets, forming a concave surface around the perimeter of the stack and a thicker Sn layer in the center. The joint microstructure was investigated using a polarized light microscope and Zeiss Auriga scanning electron microscope (SEM) with an EBSD detector to determine the orientation and size of the Sn solder grains and an energy-dispersive x-ray detector (EDS) for compositional analysis. TSL OIM Data Collection and Analysis software were used to gather the EBSD patterns and create OIM maps.

Once single and bicrystal regions larger than 500 µm were identified, one half of the solder stack was sectioned into rectangular solder bars 500 µm wide, 500 µm thick, and 4.25 mm long by electrical discharge machining (EDM). The bars were mechanically polished to a cross-section area of 300 µm by 300 µm to remove any surface damage induced by EDM. EBSD mapping was done on the front surface of the solder bars to confirm the grain orientation and size, as shown in Fig. 1 (b) and (c). EBSD mapping of the sides of several solder bars confirmed that the horizontal grain boundaries extended through the width of the samples.

IMC growth due to thermal aging and EM depends on Cu diffusion. Interstitial diffusion of Cu in Sn is highly anisotropic with the fastest diffusion direction along the c-axis of the Sn grain. The solder bars were ranked from slowest to fastest diffusion by comparing the angle between the c-axis of the β-Sn grain and a

vector normal to the Cu/solder interfacial plane, the θ angle. Six samples were selected for testing, three for thermal aging and three for EM testing. Each sample set contains a slower diffusion sample with a large θ angle, a faster diffusion sample with a smaller θ angle, and a bicrystal sample containing a small θ angle grain and a large θ angle grain, shown in Fig. 2. Specific θ angles are summarized in Table 1.

EM testing was done at a current density of 1×10^4 A/cm^2 for 100 h. The testing fixture was placed inside an insulated box furnace and heated to 140 °C to avoid temperature fluctuations due to resistive heating. If the sample thermocouple indicated a temperature increase beyond 140 °C, forced-air cooling was applied to restabilize the temperature. Lab-scale x-ray microtomography (Zeiss 520 Versa) was done before and after EM testing in order to analyze and quantify IMC and void growth. The tomography scans were first filtered in ImageJ to increase contrast and remove noise and then segmented in Avizo 9 (ThermoFisher Scientific, Waltham, MA, USA) to create 3D volume renderings for analysis and visualization. Thermal aging was done at 140 °C for 100 h in order to compare the microstructural changes driven by current flow and those driven by thermal diffusion. Since the thermal aging samples would not experience temperature fluctuations that would require application of additional cooling or heating methods, these samples could be tested in a vacuum chamber. After testing, samples were imaged in the SEM and scanned using x-ray tomography before being mounted in epoxy and mechanically polished to 0.05 μm colloidal silica finish. The mounted samples were analyzed in the SEM using EBSD and EDS to determine changes in grain structure and composition.

3. Results

3.1. Solder joint surface evolution

The six solder joints were imaged in the SEM before and after testing, as shown in Fig. 3. The faster diffusion and bicrystal EM-tested samples exhibited severe surface deformation and consumption of the Cu anode. The slower diffusion EM-tested sample and the thermally aged samples maintained planar faces similar to their as-fabricated condition. Of the thermally aged samples, only the faster diffusion sample, Fig. 3(k), showed surface relief, in the form of fine teardrop protrusions from the sample surface. Focused ion beam (FIB) cross sectioning revealed these protrusions to be second phase particles underneath a thin Sn surface layer. After very light polishing, EDS analysis confirmed that the particles were Cu_6Sn_5 IMC that coarsened during aging. Each of the EM-tested samples had a different characteristic surface morphology after testing, illustrated in Fig. 4. The slower diffusion sample showed teardrop patterns similar to the faster diffusion sample in the thermal aging set, although not as extended from the sample surface, resembling Sn hillocks seen by Chen et al. [11] and Tian et al. [17] during EM testing of solder bumps. The difference in protrusion height is potentially due to the formation of a more tenacious surface oxide on the EM sample, as the EM testing was conducted in air while the thermal aging was done in vacuum. As with the thermally aged sample, these teardrops are caused by IMCs coarsening at and slightly beneath the sample surface. The faster diffusion sample in the EM set experienced major degradation with the surface rippling and cracking in the vicinity of the ripples. The Cu anode consumption is evident from the SEM images, particularly in the bottom right corner of the joint where it appears to have crumpled inward as the Cu diffused away from the anode interface. Inspection of the bicrystal sample revealed evidence of Cu_6Sn_5 hexagonal needles, formed close enough to the sample surface to be visible in multiple locations, highlighted by white arrows in Fig. 4 (d). These needles are unique to the bicrystal EM-tested sample and were not seen on any others.

3.2. IMC growth

Cu_6Sn_5 and Cu_3Sn IMCs form when Sn-rich solders in contact with Cu substrates undergo reflow, thermal aging, and EM. In order to characterize the morphology and distribution of IMC particles in the solder bulk, the solder bars were scanned using x-ray microtomography before and after EM testing. The thermally aged bars were only scanned after aging. X-ray microtomography nondestructively captures 3D structural information based on density, as x-rays will attenuate differently based on the density of the materials they pass through. Phases with higher densities appear brighter and lower densities darker, allowing for differentiation between Cu, tin, IMCs, and void space. This technique enables quantification and visualization of IMC and void volumes that lend unique insight into their evolution and relation to the surrounding solder matrix. Pre-testing scans revealed that there were no IMC particles in the solder bulk larger than 1 μm, i.e., the resolution of the tomography scans. SEM imaging of the sample surfaces prior to

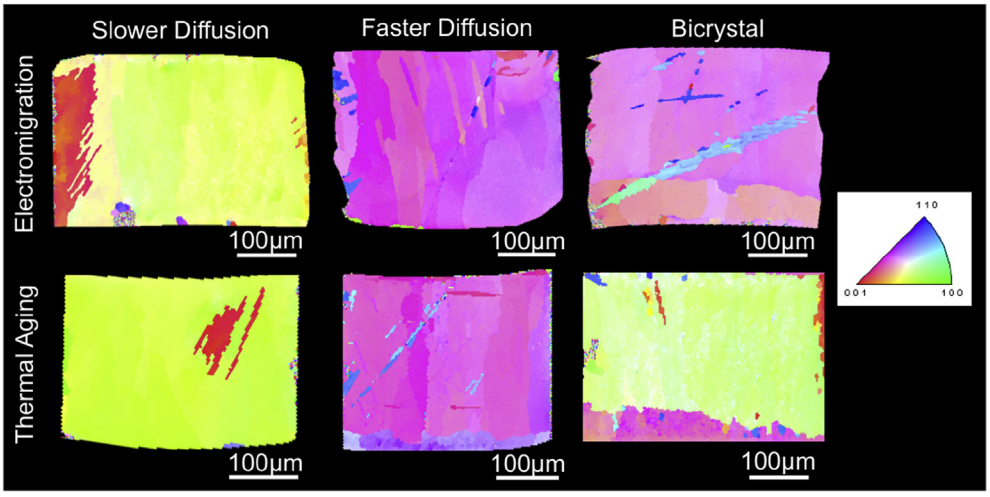

Fig. 2. OIM maps of samples selected for testing. The slower and faster diffusion samples are composed of a single grain with a predominant single orientation, while the bicrystal samples contain two grains with different orientations.

Table 1
Angles between the c-axis and electron flow direction for samples to be used in testing.

	Single Crystal Slower Diffusion	Single Crystal Faster Diffusion	Bicrystal
Electromigration Testing	72°	50°	55°/88°
Thermal Aging	76°	50°	54°/84°–86°

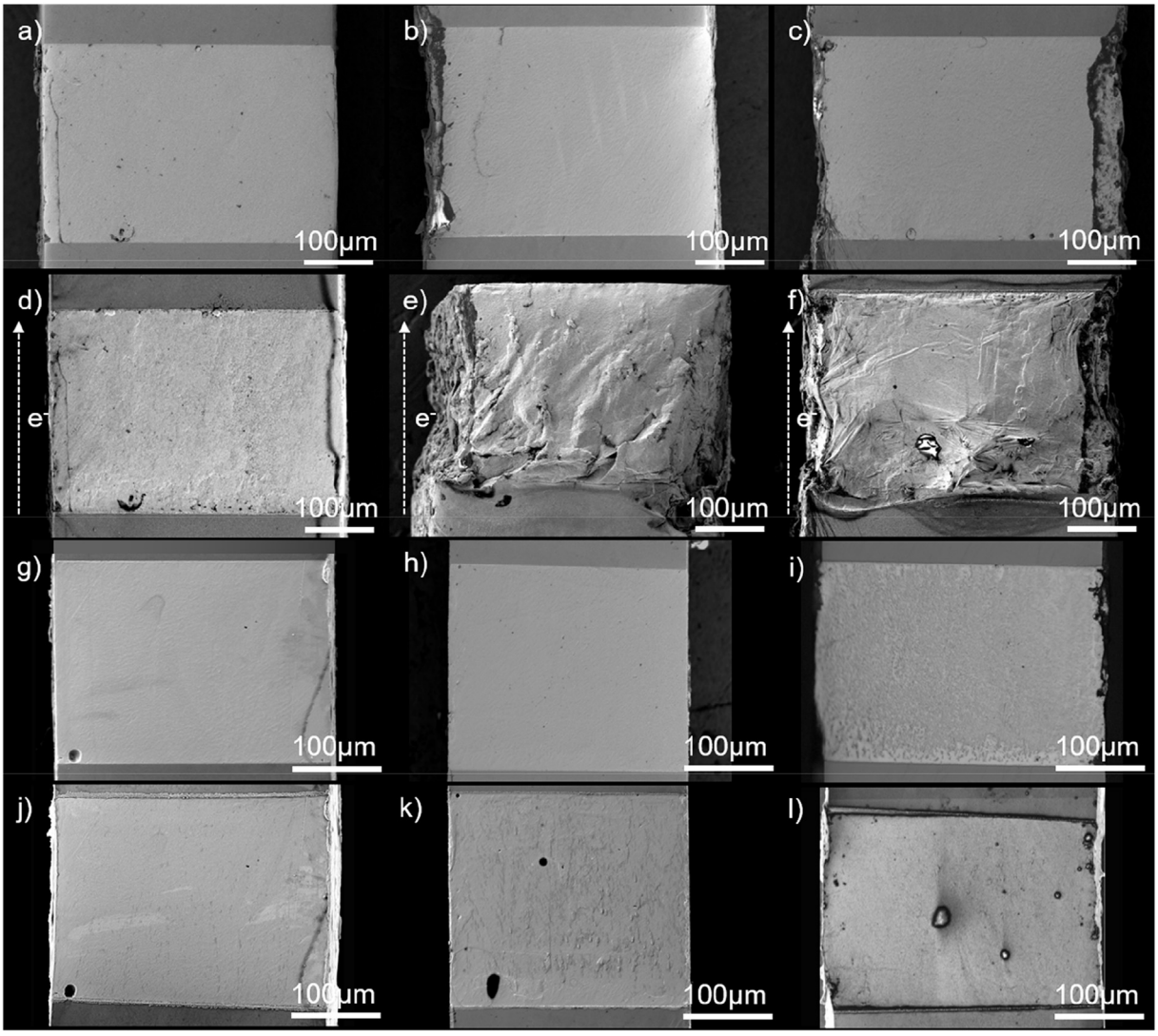

Fig. 3. SEM images of solder bar samples before and after EM testing (a–f) and thermal aging (g–l): Pre-EM (a–c), Post-EM (d–f), Pre-aging (g–i), Post-aging (h–l). Slower diffusion samples (left column), faster diffusion samples (center column) and bicrystal samples (right column) are shown. The dashed white arrow shows the electron flow direction.

testing showed finely interspersed IMC particles, the majority of which were less than 1 μm long and 0.5 μm wide. While these particles could not be captured by pre-test tomography scans, SEM analysis confirmed the size and distribution of particles to be consistent across all six samples.

Renderings of the Cu_6Sn_5 bulk IMC that grew in the EM samples are presented in Fig. 5. The IMC was determined to be Cu_6Sn_5 due to a characteristic greyscale determined in previous tomography scans. Phases are identified in tomography due to differences in density, which cause variations in x-ray intensity loss during scanning. These intensity losses translate to greyscale values in the image stack used for segmentation. Compositional analysis by EDS mapping in the SEM can confirm the which phase a greyscale corresponds to. If all imaging parameters are kept constant and samples have the same dimensions and composition, the same phase can be identified in multiple tomography scans based on greyscale. In addition, all bulk IMC particles shown in Fig. 5 were confirmed to be Cu_6Sn_5 through subsequent EDS analysis.

A significant difference in IMC growth is immediately evident from the reconstructions. The slower diffusion sample shows rod and plate-like IMC particles, the faster diffusion sample transformed almost completely into Cu_6Sn_5, and the bicrystal sample formed a dense network of rod-like IMCs. Segmentation of tomography scans in the Avizo software creates a 3D replica of the internal structure of the IMC from which volume, surface area and other features can be extracted. The accuracy of segmented tomography data relies on the pixel to micrometer ratio of the scan. The pixel to micrometer ratio for the scans used in this study were 1

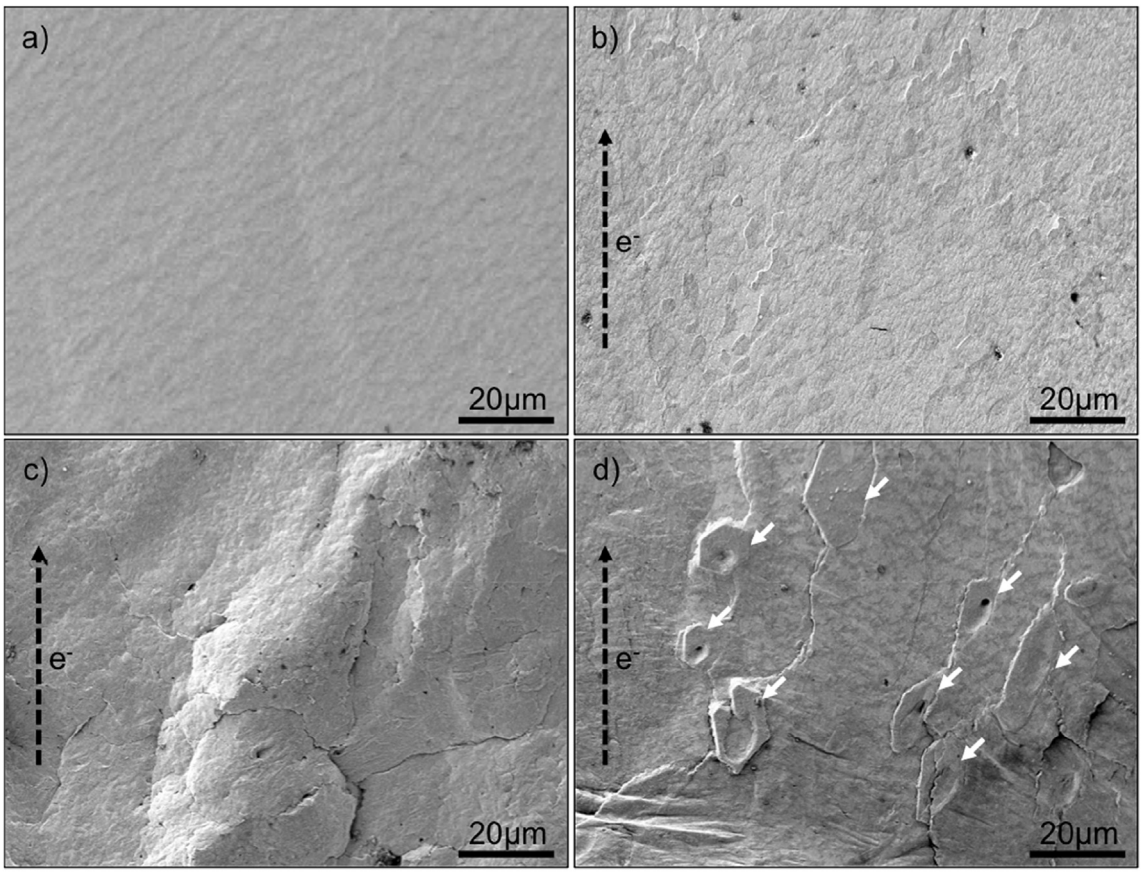

Fig. 4. SEM images of solder joint surfaces before (a) and after EM testing (b, c, d). Variations in IMC growth between the slower diffusion sample (b), faster diffusion sample (c), and the bicrystal sample (d) cause a variety of surface deformations, in particular the growth of hexagonal Cu_6Sn_5 IMC needles (indicated with white arrows) visible on the surface of (d).

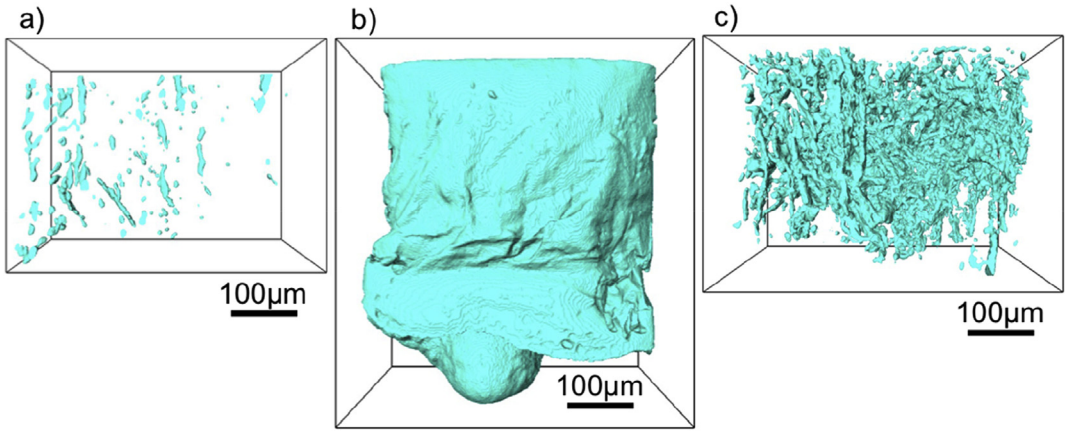

Fig. 5. IMC volume after EM for: (a) slower diffusion sample, (b) faster diffusion sample, and (c) bicrystal sample.

pixel to 1 ± 0.2 μm. A pixel in three dimensions is termed a voxel, a cube where each side length is 1 pixel. If the pixel to micrometer ratio is 1 the voxel would represent 1 μm^3. Particles with a volume of 8 voxels or less were considered noise, meaning the volumes extracted from the 3D reconstructions were accurate to approximately 9.6 μm^3. Quantification of the IMC volumes and comparison to the initial scan allowed for the calculation of an IMC growth rate for each sample, shown in Fig. 6. The faster diffusion sample grew at a rate of 202.5 μm^3/s, approximately 26 times faster than the bicrystal sample and approximately 500 times faster than the slower diffusion sample.

The thermally aged samples experienced much less IMC growth as evidenced in Fig. 7. In order to resolve the fine IMC particles in the thermal aging samples and avoid interference from interfacial voids, only the center volumes of each sample were segmented. The slower diffusion and faster diffusion single crystal samples developed an even dispersion of fine IMC particles with no difference in particle size or distribution. IMC particles in the bicrystal sample coarsened in two regions, forming elongated particles in vertical chains in the slower diffusion grain and rounded particles clustered

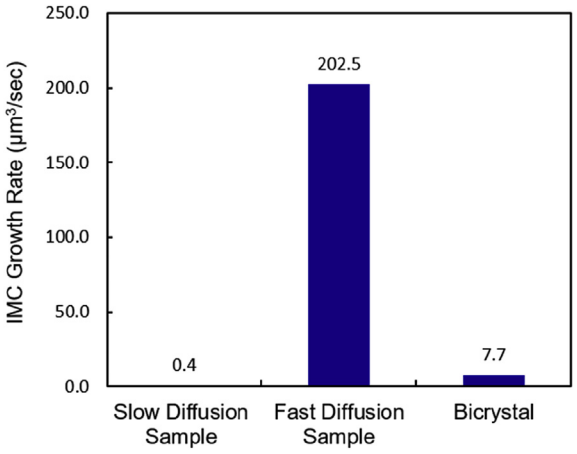

Fig. 6. IMC growth rates for each sample, showing drastically rapid IMC growth in the faster diffusion sample.

along the plane of the horizontal grain boundary. EBSD analysis of the slow diffusion grain of the bicrystal sample shows that it contains vertical subgrain boundaries. Cu diffusion would be slightly more rapid along the vertical boundaries than the surrounding matrix, causing IMC particles to nucleate and grow along these boundaries preferentially. The high angle horizontal grain boundary served as a fast diffusion pathway for Cu to migrate laterally within the sample, creating a sheet of rounded, as opposed to elongated, particles.

3.3. Grain orientation evolution

Samples were analyzed using EBSD to determine the original orientation of the β-Sn grains then repolished and analyzed again after testing. The post-testing EBSD maps reveal if and how the β-Sn grains recrystallized in response to thermal aging and EM. As shown in Fig. 8, the initial grain orientation was retained in all cases for the thermally aged samples. In contrast, the EM-tested samples experienced a range of recrystallization, seen in Fig. 9. The slower diffusion sample showed minor recrystallization in isolated patches over the joint surface. The faster diffusion sample transformed almost entirely into columnar grains of Cu_6Sn_5 that spanned the length of the joint. The bicrystal sample recrystallized entirely.

3.4. Void growth

Reconstructions of voids in the EM samples are presented in Fig. 10(a–f). As with the IMC growth, the void growth experienced by each type of sample was different. Void volumes at the anode and cathode, before and after testing, are shown in Fig. 10 (g), while anode and cathode growth rates for each sample are show in Fig. 10 (h). The slower diffusion sample had the least growth, as expected from the large θ angle. The faster diffusion sample showed rapid growth at both interfaces, while the bicrystal sample experienced rapid anode void growth, but minor cathode growth. In all cases the anode void growth surpassed that of the cathode due to the vacancy flux towards the anode caused by atomic migration towards the cathode. Void growth analysis for the thermally aged samples was not possible due to the lack of a pre-aging scan, however post-aging voids remained spherical and did not differ between cathode and anode or between samples.

4. Discussion

4.1. Thermal aging and EM comparison

Although both thermal aging and EM experiments were conducted at the same temperature and duration, their effects on solder joint microstructure were significantly different. The

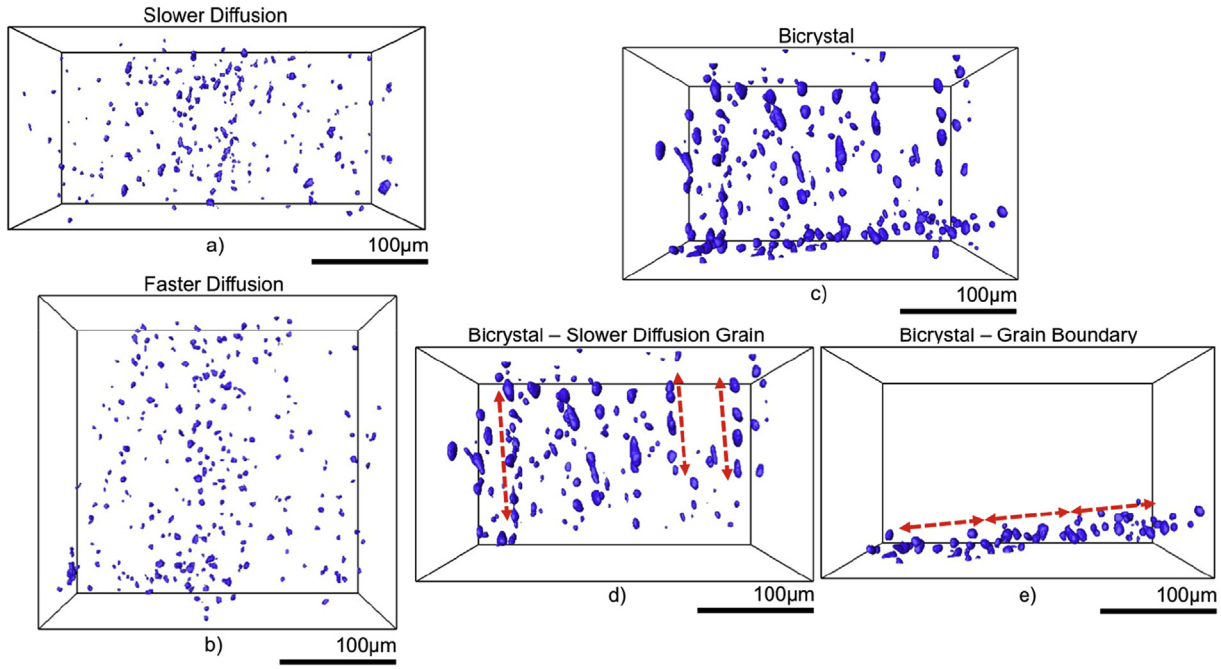

Fig. 7. IMC volumes from sample centers after thermal aging for: (a) slower diffusion sample, (b) faster diffusion sample, and (c) bicrystal sample. Two distinct IMC distributions visible in the bicrystal sample, (d) elongated particles with vertical alignment in the slower diffusion grain and (e) rounded particles that coarsened along the horizontal grain boundary. Cu diffusion directions are shown by red arrows. (For interpretation of the references to color in this figure legend, the reader is referred to the Web version of this article.)

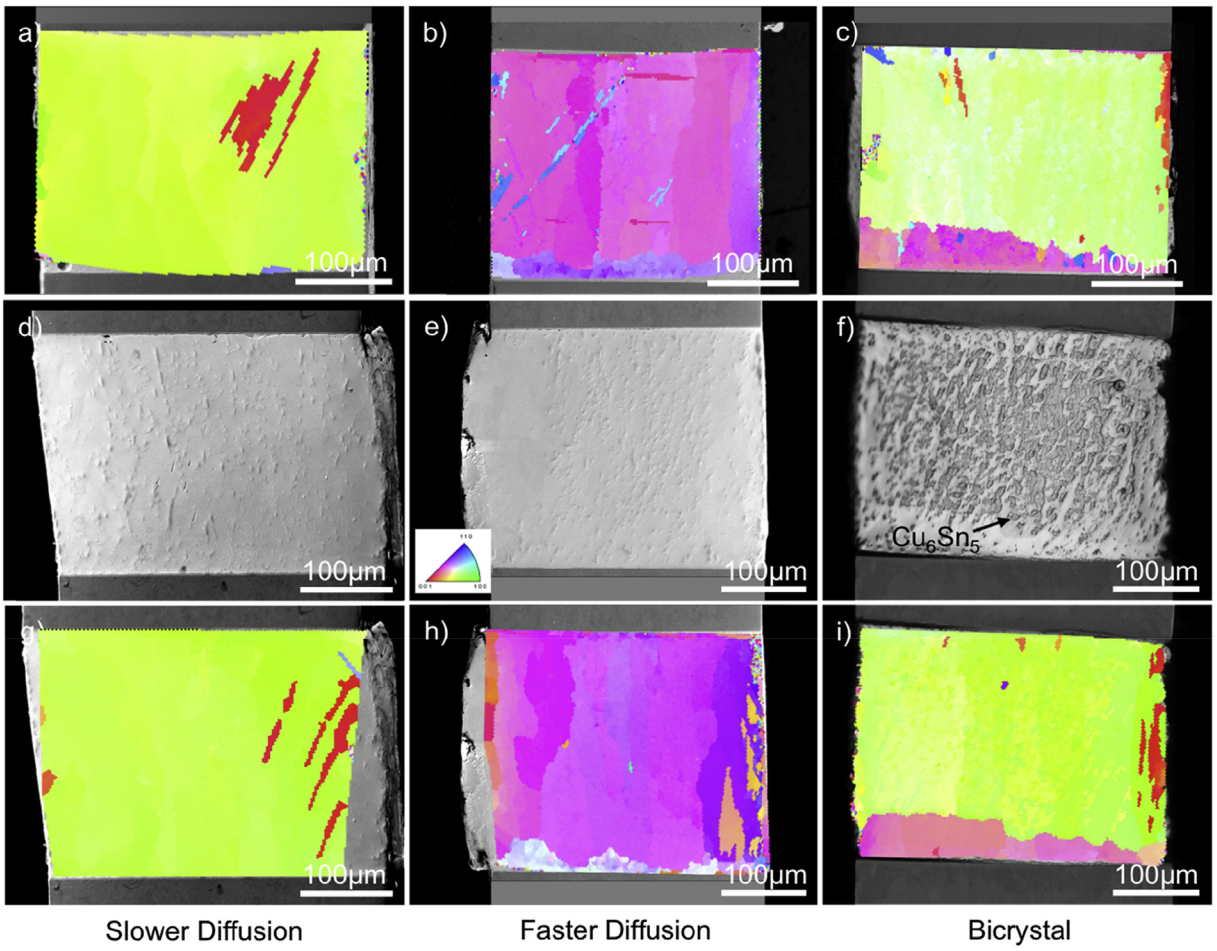

Fig. 8. SEM images and OIM maps of pre- and post-thermal aging samples showing the change in grain structure after aging: (a, b, c) pre-aging OIM maps, (d, e, f) SEM images of repolished sample surfaces after aging, (g, h, i) post-aging OIM maps.

thermal aging samples showed little surface deformation after testing and EBSD mapping showed that initial crystal orientations remained unchanged. The EM-tested samples experienced rapid IMC and void growth, which had a pronounced effect on their final microstructures. While both sets of samples had similar θ angles, the driving force for diffusion in the EM case is much higher than the in the thermal aging case. In EM, atomic diffusion is driven by both by electron momentum transfer, often called the "electron wind force," and by the chemical potential gradient created by the variation in atomic concentrations of Sn and Cu throughout the solder joint [18]. Diffusion in the thermal aging case is only driven by the chemical potential gradient and is therefore much less damaging than the EM-driven diffusion. Only the thermally aged bicrystal joint experienced appreciable IMC growth. Rounded IMC particles coarsened at the grain boundary, as Cu that diffused through the fast diffusion grain could not easily diffuse into the slower diffusion grain. Similarly, Cu diffusion in the slow diffusion grain was concentrated along subgrain boundaries and formed elongated IMC particles. The bicrystal nature of the joint lead to more IMC growth during thermal aging than in the single crystal samples where grain orientations were isolated. This suggests that in slow diffusion cases like thermal aging, grain boundary diffusion might be the controlling feature for IMC growth.

While thermal aging did not result in Sn grain structure changes or void growth, the IMC coarsening is still important to note. Isothermal aging above at 150 °C has been shown to reduce the shear strength of lead-free solder joints due to coarsening of bulk IMC particles [7,15]. Thermal cycling has proven to be significantly more damaging than thermal aging due to the build-up of plastic deformation at strained regions in the joint that then become crack nucleation sites [7]. This crack growth was captured in a 2019 study by Regalado and collaborators [19] on thermal cycling of nano-sintered silver solder. Tomography reconstructions showed the formation of a dense network of microcracks that lead to solder delamination from the substrate and substrate cracking. The relatively short timescale of these experiments (100 h), single temperature hold, and slower diffusion kinetics are why the thermally aged samples show little damage in comparison to EM-tested samples. However, comparisons between thermally cycled and power cycled joints would be an interesting direction for future work.

4.2. IMCs in EM

4.2.1. Morphology and growth

The ability to visualize the bulk IMC particles using micro-tomography was of particular interest in these experiments. In 2016 Mertens, Kirubanandham, and Chawla [20] used x-ray microtomography to capture rapid IMC growth in a solder joint after close to 500 h of EM testing. These experiments were done on polycrystalline joints so relationships between the branched IMC morphology and matrix orientation were unclear, but they proved that x-ray microtomography was a uniquely powerful tool to understand IMC growth. In our work reconstructions of the Cu_6Sn_5

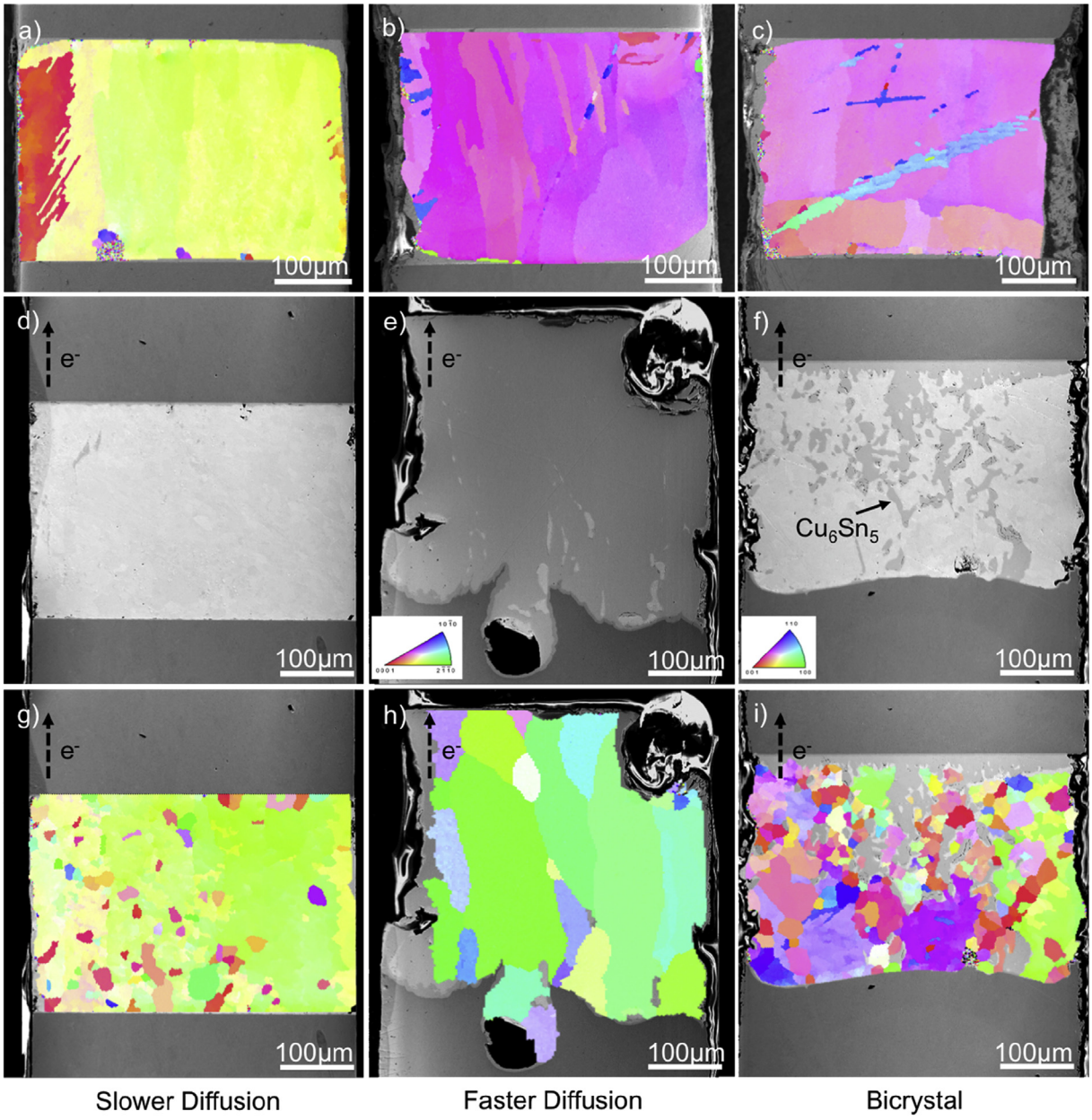

Fig. 9. SEM images and OIM maps of pre- and post-EM tested samples showing the change in grain structure after testing: (a, b, c) pre-EM OIM maps, (d, e, f) SEM images of repolished sample surfaces after testing, (g, h, i) post-EM OIM maps.

IMC from the EM-tested samples demonstrate two distinct types of IMC growth. In the slower diffusion and bicrystal samples, Cu diffuses into the solder bulk along the c-axis of the β-Sn grain and along grain boundaries where it reacts with the Sn matrix to form Cu_6Sn_5 particles. These particles gradually coarsen over time into rod or plate-like features. The second type of IMC growth is seen in the faster diffusion sample, where Cu diffused to the cathode instead of building up in the solder bulk. The cathode interfacial Cu_6Sn_5 layer grew rapidly towards the anode in large columns instead of forming IMC particles in the solder bulk.

These two types of IMC growth can be clearly differentiated when comparing their orientations and grain size using EBSD, shown in Fig. 11. The IMC in the faster diffusion sample is composed of less than 20 columnar grains with similar orientations. The IMC in the bicrystal sample is composed of multiple, fine grains less than 200 μm^2 in area. IMC grains close to the cathode interface tend to have an angle of less than 20° between the (0001) plane and the Cu interface and grow along the [0001] direction. Bulk IMC particles do not have any consistent orientations. The small angle between the basal plane of η-Cu_6Sn_5 and the Cu interface is consistent across multiple interfacial IMC grains, suggesting an orientation relationship between the cathode Cu and interfacial IMC. Previous work has shown that η-Cu_6Sn_5 has the following relations with Cu: $\{0001\}_{\eta\text{-IMC}}//\{011\}_{Cu}$, $\{10\bar{1}0\}_{\eta\text{-IMC}}//\{111\}_{Cu}$, and $\{11\bar{2}0\}_{\eta\text{-IMC}}//\{001\}_{Cu}$ [21–24]. Our Cu substrate has a primarily {111} texture so one would expect to see $\{10\bar{1}0\}$ planes of η-Cu_6Sn_5 growing parallel to the interface, however we do not see this orientation. This is because solder joints with polycrystalline Cu substrates, regardless of grain orientation, characteristically show Cu_6Sn_5 growth along [0001] normal to the Cu interface [12,25,26], as seen in our samples. This is likely due to crystals with the fastest growth direction, [0001], normal to the interface growing more rapidly and eclipsing

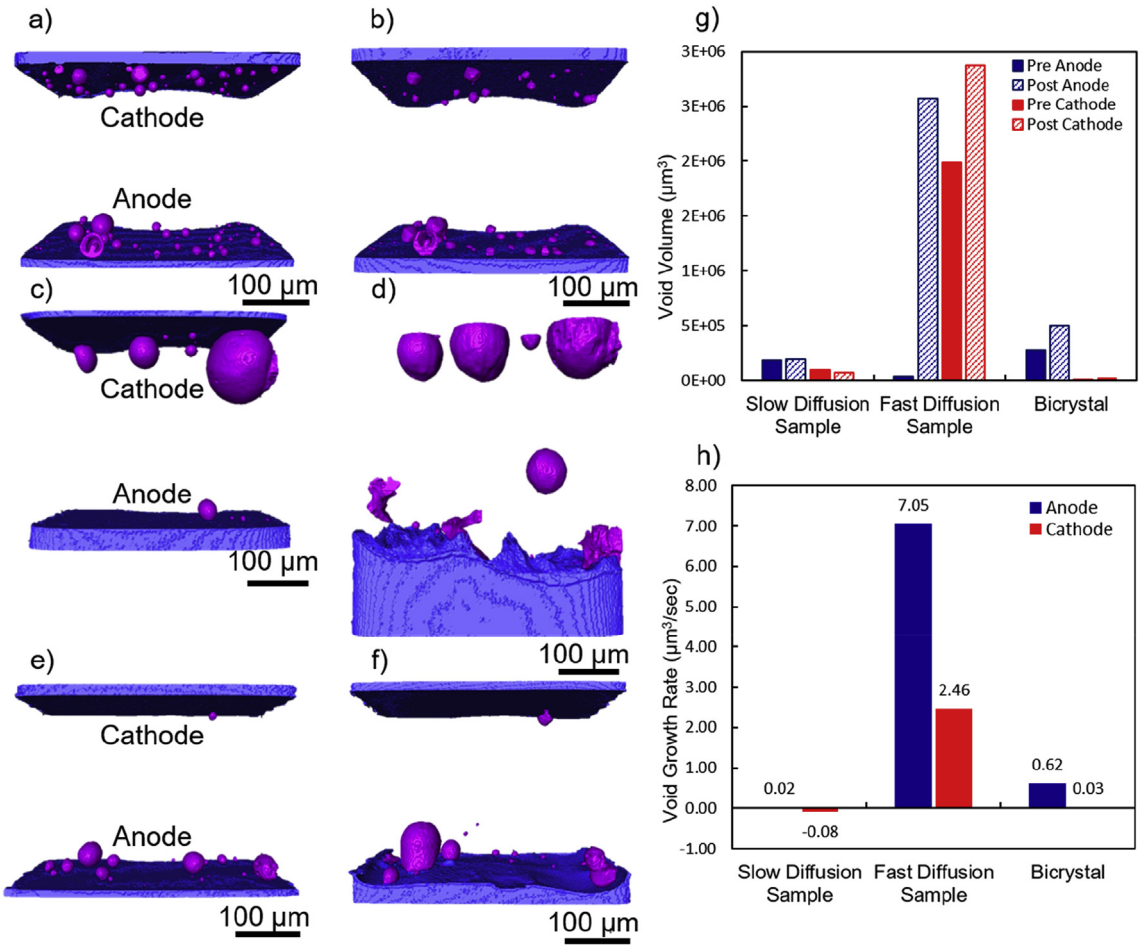

Figure 10. (a–f): Void and Cu surface volume renderings before (a, c, e) and after (b, d, f) EM testing. Volumes (a) and (b) are the slower diffusion sample, (c) and (d) are the faster diffusion sample, and (e) and (f) are the bicrystal sample. Purple represents void space and blue represents Cu. (g) Void volume change due to EM testing at the anode and cathode. (h) Void growth rate at the anode and cathode.

less favorably oriented grains early on in reflow.

The grain orientation differences between the interfacial and bulk IMC in the bicrystal sample are illustrated in Fig. 11(c) where the angle between the (0001) plane of the hexagonal Cu_6Sn_5 lattice and the Cu interface has been plotted as a function of distance from the cathode interface. The faster diffusion sample IMC has a consistent orientation of less than 30° with reference to the interface throughout the sample, meaning the IMC grew from the Cu interface towards the anode. Within 50 μm of the cathode interface the bicrystal sample IMC grains pattern off of the polycrystalline Cu and display a small angle between the basal hexagonal place and the interface. Further into the bulk of the bicrystal sample the angle between the basal plane and Cu interface is random, indicating the orientation relationship is no longer present. These bulk particles did not pattern from a Cu interface, instead they nucleated along high and low angle grain boundaries and therefore have a random crystallographic orientation. Grain boundary coarsening of IMC particles is visible in the thermally aged bicrystal in Fig. 7 (e). The EM-tested bicrystal sample experienced much more IMC growth and Sn matrix recrystallization, providing a high density of grain boundaries for Cu diffusion and IMC growth. Recrystallization caused the initial horizontal boundary, visible in the thermal bicrystal, to be lost. The grain orientation comparison, combined with the morphology difference seen in the tomography scans, supports the hypothesis that the bicrystal sample displays both interface and bulk-nucleated IMC growth. Bulk-nucleated growth results in randomly oriented η-Cu_6Sn_5 particles that are rod or plate-like and interface-nucleated growth results in columnar Cu_6Sn_5 grains with the (0001) plane parallel to the Cu interface. Bulk-nucleated IMC particles are difficult to capture in 2D surface analysis of solder joints precisely because they are mostly in the bulk of the sample and not visible. A few studies have reported IMC growth in the solder bulk, seen as hillocks protruding from polished sample cross sections [13,14,17], but none have shown the 3D structure of the particles or discussed how they might differ from interface-nucleated IMCs.

This variation in morphology and orientation has strong implications for solder joint reliability, as Cu_6Sn_5 has been shown to display anisotropic mechanical properties [27,28]. Jiang and Chawla [27] demonstrated a 20% reduction in strength and a 7% reduction in Young's modulus when comparing Cu_6Sn_5 micropillars indented perpendicular and parallel to the [0001] direction of the hexagonal crystal. If an entire joint transforms into large grains of Cu_6Sn_5 with similar orientations a crack would easily propagate through the joint along the (0001) planes. This type of fracture occurred during post-EM handling of the faster diffusion sample as the fully transformed joint was very brittle. Imaging and EBSD mapping of the fracture surface conducted in the SEM showed a transgranular cleavage fracture that propagated along (0001) planes, parallel and adjacent to the Cu/solder interface. In contrast, disconnected IMC particles would slow crack growth. Since the particles are randomly orientated, the basal planes will not align, making it difficult for a

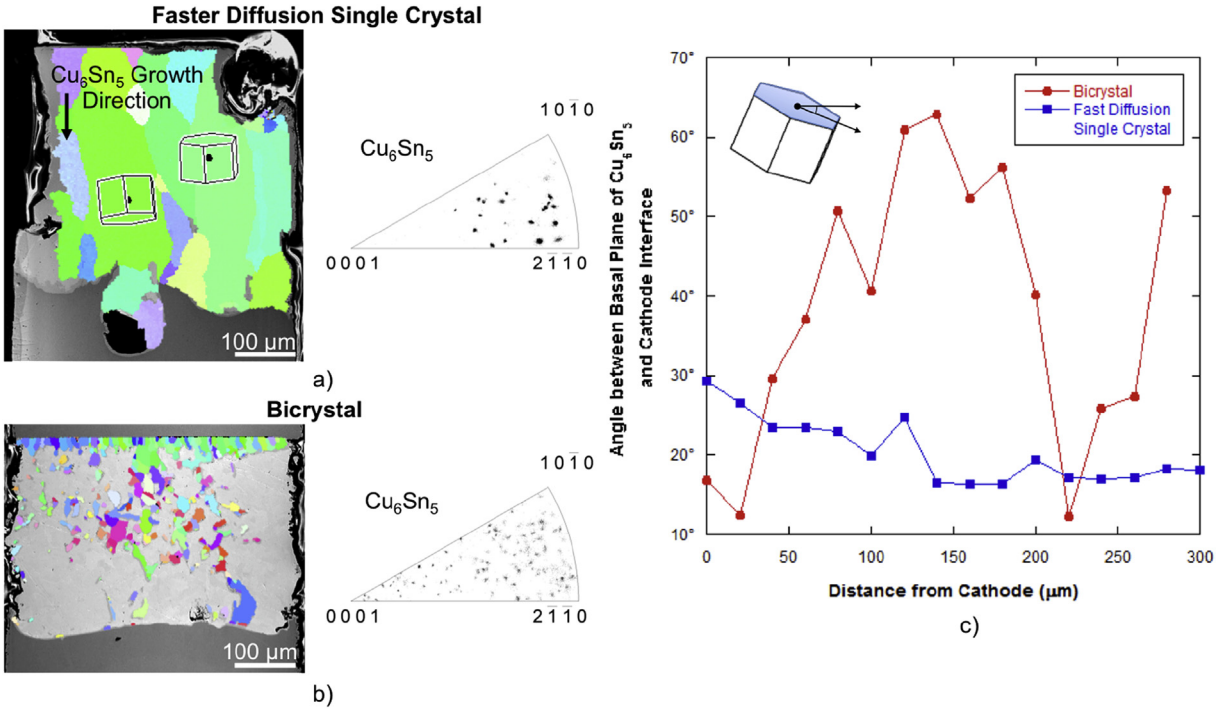

Fig. 11. Difference Cu_6Sn_5 IMC growth in the faster diffusion sample (a) and bicrystal sample (b) shown both by EBSD maps, IPF's, and plotting the angle between the basal plane and the Cu interface (c).

crack to jump into a neighboring particle. If multiple IMC rods fractured, the crack would still have to proceed through the ductile Sn matrix before complete failure could occur. In this manner, the slower diffusion and bicrystal samples would be more resistant to crack propagation than the faster diffusion sample.

4.2.2. Relationship to Sn matrix recrystallization

Bulk-nucleated IMC particle growth was seen in both the slower diffusion and bicrystal samples. The bicrystal sample exhibited complete recrystallization of the β-Sn matrix and the formation of an interconnected IMC network. The slower diffusion sample showed regions of recrystallization and isolated IMC particles. We believe that a cyclical process links matrix recrystallization and the tortuous IMC morphology. The slower diffusion sample displays an early part of the cycle while the bicrystal sample is a later stage. As IMC particles form and coarsen in the solder bulk, they impose stress on the surrounding Sn matrix. There is a volume expansion associated with the transformation of Sn to Cu_6Sn_5 which is evident when the molar volumes of each component are compared in the following way: $\Delta V = V_{Cu6Sn5}\ (cm^3/mol) - 5V_{Sn}\ (cm^3/mol) = 35.3\ (cm^3/mol)$. The Sn matrix will recrystallize in response to the stress imposed by the expanding IMC particles and IMC provides a heterogeneous nucleation site for new Sn grains to form. This recrystallization forms new grain boundaries in the vicinity of the IMC particle. New IMC particles nucleate along the recrystallized grain boundaries due to the rapid grain boundary diffusion of Cu. Since the recrystallized grain boundaries are connected to the initial IMC particle they nucleated from, it is possible that secondary IMC particles may grow along the boundaries and eventually reconnect with the original particle. In this manner, originally disconnect particles could become connected, forming the network visible in tomography and EBSD analysis of the bicrystal sample. Over time, the cycle of IMC growth and matrix recrystallization causes the entire solder joint to recrystallize and form a dense interconnected network of IMC particles. The IMC growth/recrystallization cycle is shown schematically in Fig. 12 (c).

Early and late stages of this process can be seen in Fig. 12 where we compare recrystallization in the slower diffusion and bicrystal samples. The slower diffusion sample shows the early stages of IMC growth and recrystallization. First, IMC particles (outlined in black) coarsen along the low angle subgrain boundaries, shown in blue in Fig. 12(b), (i) and (ii). The fastest IMC growth direction, the [0001] direction, is aligned with the vertical boundaries. Recrystallized Sn grains, shown numbered 1–5 in Fig. 12(b) (i) and (iii), form in response to the IMC growth and surround the IMC particles. The bicrystal sample shows the late stage of this process, where the majority of the joint has recrystallized. Fig. 12(e) shows an EBSD map color-coded by grain maximum Feret diameter with blue grains being the smallest and red the largest. The maximum Feret diameter is the longest distance between any two points along the boundary of a shape, similar to how one would measure the maximum diameter of a shape using calipers. Sn matrix grains surrounding the IMC network are blue or green (small), while those farthest away from the network are red and orange (large). This supports the idea of a continuous recrystallization process where recrystallized grains grow and finer grains nucleate within them where they contact the IMC particles, leading to a gradient in grain size. While recrystallization also took place in the faster diffusion sample, it was not driven by the same cyclic process, since the EBSD map of that sample indicates the IMC grew as a series of columns that nucleated at cathode interface and consumed the matrix Sn between them as the columns coarsened.

It is well known that solder recrystallizes under thermo-mechanical stresses, like those seen in thermal and power cycling of microelectronic packages. This recrystallization occurs in localized zones of high strain and temperature due to coefficient of thermal expansion (CTE) mismatches between packaging components and Joule heating caused by current crowding at the solder-metallization interface [29–34]. In contrast to most solder studies that use either prefabricated packages or solder bumps, the

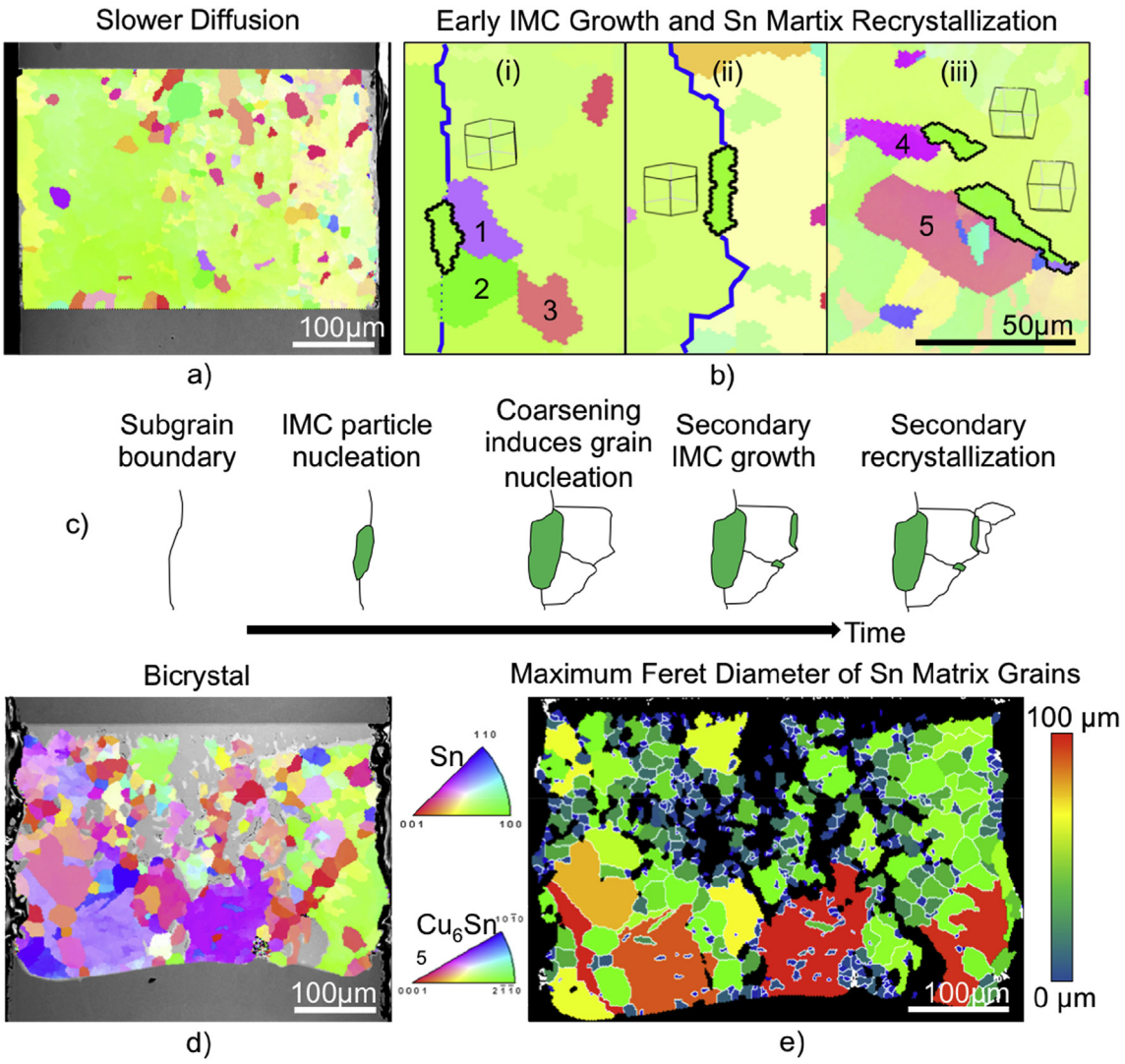

Fig. 12. IMC PSN Recrystallization in the slower diffusion sample (a,b) and bicrystal sample (d,e) with recrystallization schematic shown in (c). Magnified regions (b) of the post-EM EBSD map (a) show recrystallized Sn grains (numbered 1–5) and Cu_6Sn_5 IMC particles (outlined in black) along subgrain boundaries (lined in blue). The orientation of the IMC particles is shown using the hexagonal lattice insets. Late-stage recrystallization of the bicrystal sample is shown in (d), where the EBSD map is recolored to show maximum Feret diameter, smallest grains in blue, largest in red, and grain boundaries in white. (For interpretation of the references to color in this figure legend, the reader is referred to the Web version of this article.)

samples in this study have a uniform cross-sectional area across the length of the joint. They are also not attached to a printed circuit board (PCB) or silicon die that could impose stress on the sample during testing. This means that there are no regions of localized stress or joule heating due to sample geometry and the test configuration ensures a stable temperature so the recrystallization must occur due to stress generated within the sample.

Recrystallization through particle stimulated nucleation (PSN) of new grains has been discussed in the context of grain refinement after cold work and annealing where there is a high density of dislocations surrounding a particle which upon annealing nucleates new highly misoriented grains [31,35]. In this study, the only source of dislocation pile-up would be the coarsening bulk Cu_6Sn_5 particles, making them a logical nucleation site for new grains. However, PSN has not been explored as a recrystallization mechanism in solder EM studies, possibly for the following reasons: localized strain or heating zones, difficulty comparing initial and final grain orientations, and use of solder alloys with a range of IMC particle sizes. Strains generated by CTE mismatch between board components, joule heating, or implied mechanical force will affect the entire solder volume and therefore dwarf highly localized strains around IMC particles. Logically a sample would recrystallize in the region with highest strain, around a solder bump neck for example, and PSN recrystallization can only be seen when other strains have been eliminated.

A large focus of this study was the comparison initial and final grain orientations through EBSD and visualization of 3D microstructure using x-ray microtomography. EBSD comparison before and after testing is not by itself unique. By comparing EBSD maps before and after testing, Chen et al. [36] showed Sn grain rotation in a solder bump neck due to current crowding and strain during EM. Telang and Bieler [5,6] showed grain coarsening and orientation trends in SnAg solder under isothermal aging, creep, and thermo-mechanical fatigue. However, the combination of EBSD and tomography is particularly powerful because it connects the evolution of the 2D grain structure with the 3D structure of the solder joint, without damage that could be induced during serial sectioning. Rendering the IMC network in 3D allowed us to see

similarities and differences in growth between the three samples, not immediately evident through EBSD analysis. While the slower diffusion and bicrystal samples had very different final EBSD maps, their rod and plate-like IMC structures seen in tomography suggested they showed two stages of the same type of IMC growth. The connection between PSN recrystallization and its enhancement of further IMC growth was only made possible by using both techniques in tandem. Meanwhile, EBSD and tomography of the faster diffusion sample confirmed that it experienced a distinctly different form of IMC growth from the other two samples. Finally, the use of a simple Sn-Cu system without Ag_3Sn precipitates may have allowed this type of recrystallization to proceed more rapidly, as Ag_3Sn precipitates have been shown to pin grain boundaries and delay recrystallization in creep and thermal fatigue studies [37–39]. The combination of a sample geometry without stress concentrations, rapid IMC coarsening, comprehensive pre and post-test analysis, and a simple two element system may have made it possible to see PSN recrystallization in the context of EM where it had not been seen before.

4.3. Void growth and morphology during EM

Voids are a consistent concern in solder joint reliability since void growth can cause open circuit failure and joint embrittlement [1,2]. Voids formed due to EM have been described as pancake-like voids [40–48], finger or slit-like voids [49–51], or discrete spherical voids [44]. Pancake-like voids nucleate at current-crowding locations in the solder joint and propagate across the solder-metallization interface, while finger or slit-like voids are formed due to void growth along the current flow direction or collapse of spherical voids [17,50,53]. The type of void that develops is dependent on current-crowding, joint geometry, and, as we will show, local grain orientation.

Voids can be present in as-fabricated samples due to imperfect contact between the solder and metallization layer or due to reacting flux that becomes gaseous during reflow and cannot escape the liquid solder [54,55]. Since these voids are bubbles in the liquid solder all voids are initially spherical and typically in contact with a solder/metallization interface, as visible in Fig. 10 (a, c, e). Since void growth during EM is driven by vacancy diffusion it will be affected by current crowding, joule heating, and local grain orientation. The most commonly described void type is pancake voiding, where a single void nucleates at the corner of a solder joint due to current crowding and joule heating and propagates along the solder/metallization interface, eventually causing failure. As discussed above, our sample geometry does not display current crowding or joule heating effects due to a constant cross-sectional area throughout the sample, and as a result, the void growth seen in the solder bars is significantly different from pancake voiding. It more closely follows the nucleation, growth, and coalescence of discrete spherical voids described by Chang et al. [43] who analyzed EM voids using 3D laminography [44]. Xie et al. [48] also visualized void growth due to EM using x-ray microtomography and reported rapid void growth at the anode within 100 h of testing. However, we see two additional void behaviors not previously shown in EM literature: void faceting and burrowing, as described in the following two sections.

4.3.1. Void faceting

The phenomenon of void faceting has been described in a series of simulation papers as the formation of flat faces driven by variations in adatom diffusivity on various crystallographic planes present on the void surface [56,57]. To the best of the authors' knowledge experimental verification of this phenomena has yet to be reported. It is known from basic crystallographic thermodynamics that surface diffusion will vary with crystallographic orientation due to the difference in atomic arrangement, and therefore binding energy, along different crystallographic planes [58]. A material with anisotropic diffusion properties undergoing significant atomic diffusion would be expected to show preferential diffusion along certain directions not only in the bulk of the material, but also along the surfaces of voids present within it. Variations in surface diffusion along different crystallographic planes in β-Sn have been shown by several studies [59–61]. However, many papers simulating void evolution under current and temperature stressing have ignored crystallographic effects and therefore have discussed void coalescence, fracture, and migration only in the context of spherical, elliptical or cardioid voids [41–43,51–53,62,63].

The combination of high current density and the anisotropic diffusion properties of β-Sn, isolated in single crystal joints in our study, drove certain spherical voids to develop flat, faceted surfaces. The degree of faceting was analyzed by quantifying the initial and final void sphericities. Sphericity is the ratio between the surface area of a perfect sphere with the same volume as a specific void to the surface area of the actual void. If the void is perfectly spherical, its sphericity will be 1, while a cuboidal void has a sphericity of approximately 0.806, a deviation of 0.19 from a sphere. Deviations from sphericity for voids before and after EM testing are shown in Fig. 13, together with reconstructions of representative voids before and after testing. Three trends are clearly visible: (i) voids in the slower diffusion sample show the greatest deviation from sphericity because they have become faceted, (ii) most voids in the faster diffusion sample have remained spherical, and (iii) the bicrystal sample shows both faceting and spherical growth at cathode and anode respectively. The mixed-mode void growth in the bicrystal sample is due to the orientation of the grain surrounding the voids at each interface. The anode voids are surrounded by a faster diffusion grain with a lower θ angle, similar to the faster diffusion sample (55° and 50° respectively). Therefore, the anode voids preserve their spherical shape, while the cathode void is surrounded by a high θ angle grain similar to the slower diffusion sample (88° and 72° respectively) and exhibits void faceting.

While it is unclear how rapidly the bicrystal sample recrystallized, it can be presumed that the PSN-recrystallization began in the bulk of the sample and spread towards the edges over time, leaving the interfacial voids unaffected in the initial stages of the EM test. Recrystallization would have destroyed the original orientation relationships and θ angles. Since the void morphologies match the original orientations, they must have evolved before recrystallization reached the interfaces. This suggests a sequential microstructure evolution where voids change shape early in EM stressing, followed by recrystallization of the surrounding matrix and IMC growth. Voids initially present at both interfaces disappeared after testing, but their disappearance did not follow clear trends with void size, spacing, or interfacial density. Investigation into how surrounding voids behave after a void disappears will determine if the void collapsed due to backfill by Sn [64] or IMC or if the voids coalesced. If the voids coalesced a neighboring void should increase in volume, while if a void collapsed the neighboring voids would remain at a constant volume.

Simulations suggest that the deciding factor that controls whether a void will remain spherical or form facets is the relationship between EM-driven surface diffusion and crystallographically-driven anisotropic surface diffusion [50,56,65]. When EM-driven diffusion is rapid, as in the case of the faster diffusion sample with a small θ angle, a void will maintain a spherical equilibrium shape. When EM-driven diffusion is slower, due to a large θ angle, anisotropic surface diffusion dominates

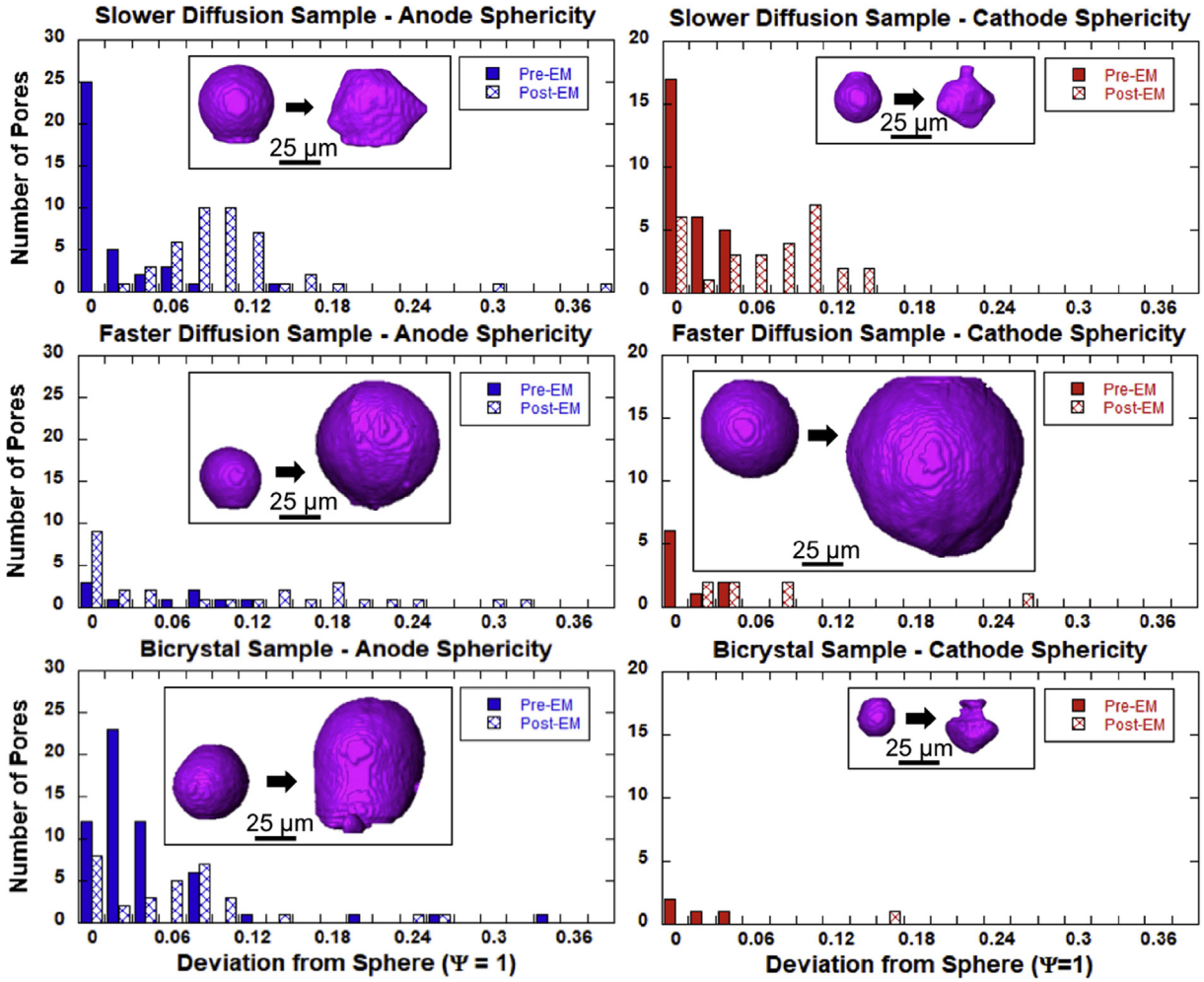

Fig. 13. Histograms showing deviation of sphericity in anode and cathode voids before and after EM testing. Deviation from sphericity is determined by the following: $\Psi_{perfect\ sphere} - \Psi_{void}$. Reconstructions of a representative void before and after testing are shown in the insets. Void faceting is evident in the slower diffusion sample and cathode of the bicrystal sample, while voids remain spherical in the faster diffusion sample and anode of the bicrystal sample.

causing voids to facet along low surface energy crystallographic planes. In β-Sn the (100) and (211) surfaces have the lowest surface energy, making growth along those planes energetically favorable [60,61]. Therefore, it is likely that the voids in the slower diffusion sample and at the cathode of the bicrystal sample formed facets along those planes. Belyakov et al. [66] reported crystallographically faceted void formation in several lead-free solder alloys subjected to thermal aging. These void facets appear to have a relationship to the β-Sn matrix orientation and grew in a layered fashion, but further relationships with crystallography were not expanded upon. The voids were faceted in both the as soldered and post aging conditions and appeared related to bulk Ag_3Sn and Cu_6Sn_5 IMC particles. In contrast, our samples show a transition from spherical to faceted based on clearly defined differences in diffusion due to EM and anisotropic surface energy effects and are not related to IMC particles, as confirmed by tomography and SEM analysis. Voids in the thermal aging cases did not exhibit faceting within 100 h, likely due to the slower diffusion kinetics, but might exhibit the phenomenon with longer testing. Further analysis of the relationships between local crystallography and void faceting are in progress.

4.3.2. Void burrowing

The second unique void behavior seen in our samples is void burrowing. Void burrowing refers to the rapid consumption of Cu surrounding a void causing it to migrate or "burrow" into the Cu interface at an unusually rapid rate compared to the rest of the sample interface. The result is massive localized Cu consumption and void migration opposite the electron flow direction. This behavior only occurred in the faster diffusion sample where interstitial Cu diffusion was expected to be rapid and at the anode interface with the fewest initial voids, visible in Fig. 14(a). Current density in the vicinity of a void is higher than the average cross-sectional current density of the solder joint due to a local reduction in cross-sectional area [44,46,48]. This causes current crowding around voids and increased atomic diffusion. Fig. 14(d)) and e) show the early stages of this type of void growth at the bicrystal anode which was surrounded by a fast diffusion grain. Rapid Cu diffusion around the void edge causes the void to develop a ridge around the bottom, with a dimple in the middle. The dimple is the result of the void preventing Cu diffusion directly along the electron flow; instead Cu atoms beneath the void must diffuse around it before being able to travel into the solder bulk. This causes a reduction in Cu dissolution right beneath pores and creates small Cu peaks, visible in blue in Fig. 14(e)). These Cu peaks correspond to the dimples seen at the base of the void in Fig. 14(d)). The faster diffusion sample likely experienced a similar type of void growth initially, with the difference that the burrowing void nucleated at

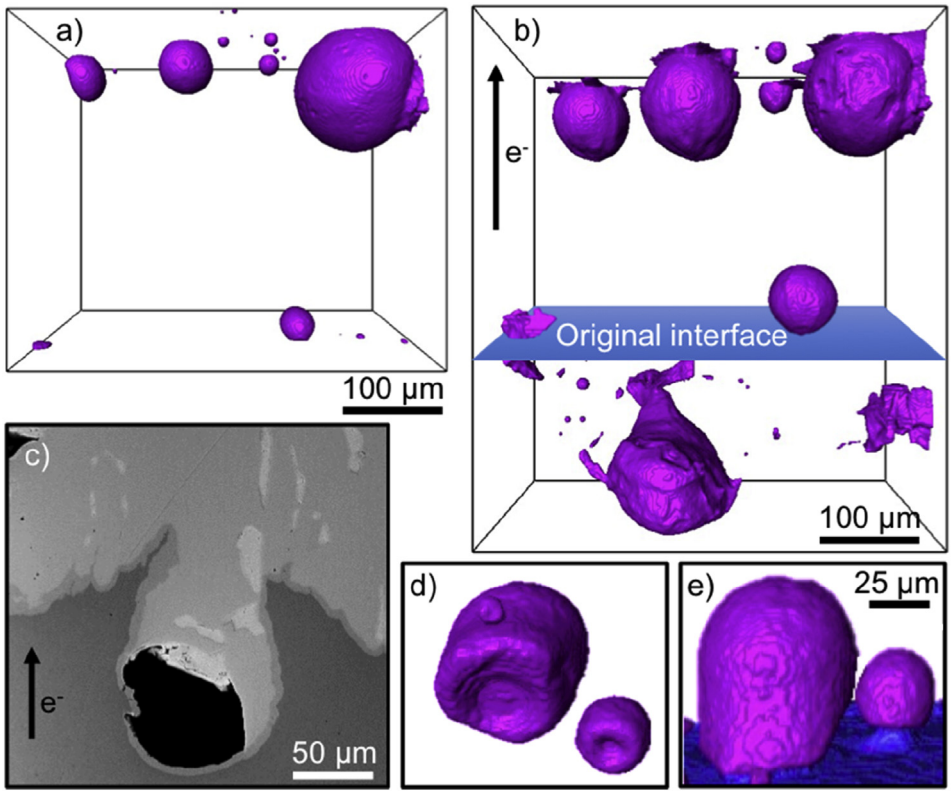

Fig. 14. Void burrowing shown by void reconstructions of the faster diffusion sample before and after EM testing (a and b), SEM image of polished sample cross-section showing burrowed void (c), and dimpled bicrystal anode voids showing rapid Cu dissolution around void edge and Cu peak beneath the voids (d and e).

the interface instead of being present in the as-reflowed condition.

Several features appear to have caused the burrowing behavior. The low θ angle of the grain ensured rapid Cu diffusion and the single crystal nature of the joint ensured that there were no barriers present to hinder diffusion in the sample bulk. While the initial anode surface being nearly void-free might suggest that the interface would experience planar consumption, we see instead that a distribution of voids across the interface ensures a uniform increase in current density across the anode interface [48] and therefore more planar Cu consumption. Nucleation of an isolated void lead to current crowding in the center of the interface and rapid diffusion close to the void. It is interesting to note that the single preexisting anode void in the faster diffusion sample did not burrow into the interface and instead expanded and remained at the same position in the solder matrix. The final detail that may have encouraged void burrowing is the excess of Cu provided by the Cu bars attached to the solder. Had the Cu interface instead been a thin metallization layer, the void would have propagated along the Cu interface in a pancake-voiding fashion as it progressively consumed the Cu layer [64]. With an unlimited Cu supply and lack of current crowding due to sample geometry, the void was free to propagate directly into the Cu bar.

5. Conclusions

The purpose of this work was two-fold; first, to compare microstructural evolution due to thermal aging and EM done at the same temperature and second, to evaluate those microstructural changes using tomography to visualize and quantify IMC and void growth and EBSD to determine changes in crystallography. We reached the following conclusions.

- Two sets of single crystal and bicrystal solder joints were fabricated with a range of comparable grain orientations. One set was thermally aged for 100 h at 140 °C and the second set was EM tested for 100 h at 140 °C under a current density of 1×10^4 A/cm^2.
- SEM and microtomography analysis allowed for visualization and quantification of IMC growth, grain orientation evolution, and void growth.
- Thermally aged samples did not exhibit grain recrystallization or significant IMC particle growth after aging for 100 h. EM-tested solder joint evolution varied significantly between slower diffusion, faster diffusion, and bicrystal samples.
- Two IMC growth processes were discussed: cathode-nucleated columnar Cu_6Sn_5 growth and bulk-nucleated rod-like Cu_6Sn_5 growth.
- Bulk-nucleated growth of IMC particles was related to β-Sn matrix recrystallization by PSN recrystallization theory, not previously addressed in the context of EM.
- Two unique voiding behaviors were examined: void faceting and void burrowing. Void faceting is controlled by anisotropic atomic surface diffusion and is seen in the slower diffusion sample and bicrystal cathode due to large θ angles and slow EM-driven diffusion. Void burrowing occurred in faster diffusion sample due to rapid EM-driven diffusion, current crowding at void edges, and unlimited Cu at the anode interface.

This research shows that solder joint evolution under EM is a complex problem that requires a multidimensional analysis approach to understand. The most obvious solution to reduce EM-driven damage is a single crystal solder joint with the c-axis perpendicular to the electron flow, but as we've shown, that might only be a short-term cure. PSN recrystallization at subgrain

boundaries will cause an increase in grain boundary density and loss of the original orientation. Slow diffusion grains might also show void faceting, creating regions of localized stress leading to crack initiation. IMC growth, void growth, and matrix orientation evolution are interrelated phenomena that should be considered together when trying to determine a future solution for EM-driven damage.

Declaration of competing interests

The authors declare that they have no known competing financial interests or personal relationships that could have appeared to influence the work reported in this paper.

Acknowledgments

The authors acknowledge funding from the National Science Foundation (NSF) under contract number CMMI-1763128 (Alexis Lewis, Program Manager) and the use of facilities at the Center for 4D Materials Science at ASU. MBK acknowledges funding from a Dean's Graduate Fellowship from the Fulton Schools of Engineering at Arizona State University, as well as an ARCS Fellowship.

Appendix A. Supplementary data

Supplementary data to this article can be found online at https://doi.org/10.1016/j.jallcom.2019.152918.

References

[1] K.N. Tu, Recent advances on electromigration in very-large-scale-integration of interconnects, J. Appl. Phys. 94 (2003) 5451, https://doi.org/10.1063/1.1611263.
[2] C. Chen, S.W. Liang, Electromigration issues in lead-free solder joints, J. Mater. Sci. Mater. Electron. 18 (2007) 259–268, https://doi.org/10.1007/s10854-006-9020-8.
[3] B.F. Dyson, T.R. Anthony, D. Turnbull, Interstitial diffusion of copper in tin, J. Appl. Phys. 38 (1967) 3408, https://doi.org/10.1063/1.2936996.
[4] A. Khosla, H.B. Huntington, Electromigration in tin single crystals, J. Phys. Chem. Solids 36 (1975) 395–399.
[5] A.U. Telang, T.R. Bieler, D.E. Mason, K.N. Subramanian, Comparisons of experimental and computed crystal rotations caused by slip in crept and thermomechanically fatigued dual-shear eutectic Sn-Ag solder joints, J. Electron. Mater. 32 (2003).
[6] A.U. Telang, T.R. Bieler, S. Choi, K.N. Subramanian, Orientation imaging studies of Sn-based electronic solder joints, J. Mater. Res. 17 (2002), https://doi.org/10.1557/JMR.2002.0337.
[7] Y.H. Lin, C.M. Tsai, Y.C. Hu, Y.L. Lin, C.R. Kao, Electromigration-induced failure in flip-chip solder joints, J. Electron. Mater. 34 (2006).
[8] Y.C. Hu, Y.H. Lin, C.R. Kao, K.N. Tu, Electromigration failure in flip chip solder joints due to rapid dissolution of copper, J. Mater. Res. 18 (2003), https://doi.org/10.1557/JMR.2003.0355.
[9] R. Rosenberg, M. Ohring, Void formation and growth during electromigration in thin films, J. Appl. Phys. 42 (1971), https://doi.org/10.1063/1.1659998.
[10] M. Lu, D.Y. Shih, P. Lauro, C. Goldsmith, D.W. Henderson, Effect of Sn grain orientation on electromigration degradation mechanism in high Sn-based Pb-free solders, Appl. Phys. Lett. 92 (2008) 211909, https://doi.org/10.1063/1.2936996.
[11] J.Q. Chen, J.D. Guo, K.L. Liu, J.K. Shang, Dependence of electromigration damage on Sn grain orientation in Sn–Ag–Cu solder joint, J. Appl. Phys. 114 (2013) 153509, https://doi.org/10.1063/1.4825323.
[12] A. Tasooji, L. Lara, K. Lee, Effect of grain boundary misorientation on electromigration in lead-FreeSolder joint, J. Electron. Mater. 43 (2014), https://doi.org/10.1007/s11664-014-3321-0.
[13] M.L. Huang, J.F. Zhao, Z.J. Zhang, N. Zhao, Role of diffusion anisotropy in β-Sn in microstructural evolution of Sn-3.0Ag-0.5Cu flip chip bumps undergoing electromigration, Acta Mater. 100 (2015) 98–106, https://doi.org/10.1016/j.actamat.2015.08.037.
[14] M.L. Huang, J.F. Zhao, Z.J. Zhang, N. Zhao, Dominant effect of high anisotropy in β-Sn grain on electromigration-induced failure mechanism in Sn-3.0Ag-0.5Cu interconnect, J. Alloy. Comp. 678 (2016) 370–374, https://doi.org/10.1016/j.jallcom.2016.04.024.
[15] X. Deng, R.S. Sidhu, P. Johnson, N. Chawla, Influence of reflow and thermal aging on the shear strength and fracture behavior of Sn-3.5Ag solder/Cu joints, Metall. Mater. Trans. A 36A (2005) 55–64.
[16] Y.A. Shen, C. Chen, Effect of Sn grain orientation on formation of Cu_6Sn_5 intermetallic compounds during electromigration, Scr. Mater. 128 (2017) 6–9, https://doi.org/10.1016/j.scriptamat.2016.09.028.
[17] Y. Tian, J. Han, L. Ma, F. Guo, The dominant effect of c-axis orientation in tin on the electromigration behaviors in tricrystal Sn-3.0Ag-0.5Cu solder joints, Microelectron. Reliab. 80 (2018) 7–13, https://doi.org/10.1016/j.microrel.2017.11.005.
[18] H. Gan, K.N. Tu, Polarity effect of electromigration on kinetics of intermetallic compound formation in Pb-free solder V-groove samples, J. Appl. Phys. 97 (2005), https://doi.org/10.1063/1.1861151.
[19] I.L. Regalado, J.J. Williams, S. Joshi, E.M. Dede, Y. Liu, N. Chawla, X-ray microtomography of thermal cycling damage in sintered nano-silver solder joints, Adv. Eng. Mater. 21 (2019), https://doi.org/10.1002/adem.201801029.
[20] J.C.E. Mertens, A. Kirubanandhan, N. Chawla, Electromigration mechanisms in Sn-0.7Cu/Cu couples by four dimensional (4D) X-ray microtomography and electron backscatter diffraction (EBSD), Acta Mater. 102 (2016) 220–230, https://doi.org/10.1016/j.actamat.2015.08.073.
[21] J.O. Suh, K.N. Tu, N. Tamura, Dramatic morphological change of scallop-type Cu6Sn5 formed on (001) single crystal copper in reaction between molten SnPb solder and Cu, Appl. Phys. Lett. 91 (2007), https://doi.org/10.1063/1.2761840.
[22] K.K. Wang, D. Gan, K.C. Hsieh, Orientation relationships, interfaces, and microstructure of η-Cu6Sn5 formed in the early-stage reaction between Cu and molten Sn, Thin Solid Films 519 (2010), https://doi.org/10.1016/j.tsf.2012.09.045.
[23] Z. Zhang, H. Cao, M. Li, Y. Yu, H. Yang, S. Yang, Three-dimensional placement rules of Cu6Sn5 textures formed on the (111)Cu and (001)Cu surfaces using electron backscattered diffraction, J. Mat. Des. 94 (2016) 280–285, https://doi.org/10.1016/j.matdes.2016.01.037.
[24] Z.H. Zhang, M.Y. Li, Z.Q. Liu, S.H. Yang, Growth characteristics and formation mechanisms of Cu6Sn5 phase at the liquid-Sn0.7Cu/(111)Cu and liquid-Sn0.7Cu/(001)Cu joint interfaces, Acta Mater. 104 (2016) 1–8, https://doi.org/10.1016/j.actamat.2015.11.034.
[25] L. Jiang, N. Chawla, Mechanical Properties of Cu6Sn5 intermetallic by micropillar compression testing, Scr. Mater. 63 (2010) 480–483, https://doi.org/10.1016/j.scriptamat.2010.05.009.
[26] M. Li, M. Yang, J. Kim, Textured growth of Cu6Sn5 grains formed at a Sn3.5Ag/Cu interface, Mater. Lett. 66 (2012) 135–137, https://doi.org/10.1016/j.matlet.2011.08.014.
[27] L. Jiang, H. Jiang, N. Chawla, The effect of crystallographic orientation on the mechanical behavior of Cu6Sn5 by micropillar compression testing, J. Electron. Mater. 41 (2012), https://doi.org/10.1007/s11664-012-2124-4.
[28] J.M. Song, B.R. Huang, C.Y. Liu, Y.S. Lai, Y.T. Chiu, T.W. Huang, Nanomechanical responses of intermetallic phase at the solder joint interface – crystal orientation and metallurgical effects, J. Mater. Sci. Eng. 534 (2012) 53–59, https://doi.org/10.1016/j.msea.2011.11.037.
[29] T.R. Bieler, H. Jiang, L.P. Lehman, T. Kirkpatrick, E.J. Cotts, Influence of Sn grain size and orientation on the thermomechanical response and reliability of Pb-free solder joints, in: Electronic Components and Technology Conference, 2006, pp. 1462–1467.
[30] F.Y. Ouyang, K.N. Tu, T.S. Lai, Effect of electromigration induced joule heating and strain on microstructural recrystallization in eutectic SnPb flip chip solder joints, J. Mater. Chem. Phys. 136 (2012) 210–218, https://doi.org/10.1016/j.matchemphys.2012.06.054.
[31] L. Yin, L. Wentlent, L. Yang, B. Arfaei, A. Oasaimeh, P. Borgesen, Recrystallization and precipitate coarsening in Pb-free solder joints during thermo-mechanical fatigue, J. Electron. Mater. 41 (2012) 241–252, https://doi.org/10.1007/s11664-011-1762-2.
[32] T. Matilla, J.K. Kivilahti, The failure mechanism of recrystallization-assisted cracking of solder interconnections. , 2012.
[33] T.R. Bieler, B. Zhou, L. Blair, A. Zamiri, P. Darbandi, F. Pourboghrat, T.K. LEE, K.C. Liu, The role of elastic and plastic anisotropy of Sn in recrystallization and damage evolution during thermal cycling in SAC305 solder joints, J. Electron. Mater. 41 (2012) 283–301, https://doi.org/10.1007/s11664-011-1811-x.
[34] J.J. Sundelin, S.T. Nurmi, T.K. Lepisto, Recrystallization behaviour of SnAgCu solder joints, J. Mater. Sci. Eng. A 474 (2008) 201–207, https://doi.org/10.1016/j.msea.2007.04.013.
[35] R.D. Doherty, D.A. Hughes, F.J. Humphreys, J.J. Jonas, D. Juul Jensen, M.E. Kassner, W.E. King, T.R. McNelley, H.J. McQueen, A.D. Rollett, Current issues in recrystallization: a review, J. Mater. Sci. Eng. 238 (1997) 219–274, 0921-5093/97.
[36] H. Chen, C. Hang, X. Fu, M. Li, Microstructure and grain orientation evolution in Sn-3.0Ag0.5Cu solder interconnects under electrical current stressing, J. Electron. Mater. 44 (2015) 3880–3887, https://doi.org/10.1007/s11664-015-3922-2.
[37] M. Kerr, N. Chawla, Creep deformation behavior of Sn–3.5Ag solder/Cu couple at small length scales, Acta Mater. 52 (2004) 4527–4535, https://doi.org/10.1016/j.actamat.2004.06.010.
[38] P. Borgesen, L. Wentlent, S. Hamasha, S. Khasawneh, S. Shirazi, D. Schmitz, T. Alghoul, C. Greene, L. Yin, A mechanistic thermal fatigue model for SnAgCu solder joints, J. Electron. Mater. 47 (2018) 2526–2544, https://doi.org/10.1007/s11664-018-6121-0.
[39] T.K. Lee, B. Zhou, L. Blair, K.C. Liu, T.R. Bieler, Sn-Ag-Cu solder joint microstructure and orientation evolution as a function of position and thermal cycles in ball grid arrays using orientation imaging microscopy, J. Electron.

Mater. 39 (2010) 2588–2597, https://doi.org/10.1007/s11664-010-1348-4.
[40] E.C.C. Yeh, W.J. Choi, K.N. Tu, P. Elenius, H. Balkan, Current-crowding-induced electromigration failure in flip chip solder joints, Appl. Phys. Lett. 80 (2002) 580, https://doi.org/10.1063/1.1432443.
[41] Y.W. Chang, S.W. Liang, C. Chen, Study of void formation due to electromigration in flip-chip solder joints using Kelvin bump probes, Appl. Phys. Lett. 89 (2006), 032103, https://doi.org/10.1063/1.2226989.
[42] L. Zhang, S. Ou, J. Huang, K.N. Tu, S. Gee, L. Nguyen, Effect of current crowding on void propagation at the interface between intermetallic compound and solder in flip chip solder joints, Appl. Phys. Lett. 88 (2006), 012106, https://doi.org/10.1063/1.2158702.
[43] Y.W. Chang, T.H. Chiang, C. Chen, Effect of void propagation on bump resistance due to electromigration in flipchip solder joints using Kelvin structure, Appl. Phys. Lett. 91 (2007) 132113, https://doi.org/10.1063/1.2790376.
[44] Y.W. Chang, Y. Cheng, L. Helfen, F. Xu, T. Tian, M. Scheel, M. Di Michiel, C. Chen, K.N. Tu, T. Baumbach, Electromigration mechanism of failure in flip-chip solder joints based on discrete void formation, Nature Sci. Reports (2017), https://doi.org/10.1038/s41598-017-06250-8.
[45] C.E. Ho, C.H. Yang, P.T. Lee, C.T. Chen, Real-time X-ray microscopy study of electromigration in microelectronic solder joints, Scr. Mater. 114 (2016) 79–83, https://doi.org/10.1016/j.scriptamat.2015.12.001.
[46] J.K. Han, D. Choi, M. Fujiyoshi, N. Chiwata, K.N. Tu, Current density redistribution from no current crowding to current crowding in Pb-free solder joints with an extremely thick Cu layer, Acta Mater. 60 (2012) 102–111, https://doi.org/10.1016/j.actamat.2011.09.023.
[47] Y.H. Lin, Y.C. Hu, C.M. Tsai, C.R. Kao, K.N. Tu, In situ observation of the void formation-and-propagation mechanism in solder joints under current-stressing, Acta Mater. 53 (2005) 2029–2035, https://doi.org/10.1016/j.actamat.2005.01.014.
[48] H.X. Xie, D. Friedman, K. Mirpuri, N. Chawla, Electromigration damage characterization in Sn-3.9Ag-0.7Cu and Sn-3.9Ag-0.7Cu-0.5Ce solder joints by three-dimensional X-ray tomography and scanning electron microscopy, J. Electron. Mater. 43 (2014), https://doi.org/10.1007/s11664-013-2667-z.
[49] T. Tian, K. Chen, A.A. MacDowell, D. Parkinson, Y.S. Lai, K.N. Tu, Quantitative X-ray microtomography study of 3-D void growth induced by electromigration in eutectic SnPb flip-chip solder joints, Scr. Mater. 65 (2011) 646–649, https://doi.org/10.1016/j.scriptamat.2011.07.002.
[50] D.R. Fridline, A.F. Bower, Influence of anisotropic surface diffusivity on electromigration induced void migration and evolution, J. Appl. Phys. 85 (1999) 3168, https://doi.org/10.1063/1.369656.
[51] W. Wang, Y. Yao, L.M. Keer, A statistical mechanics model to predict electromigration induced damage and void growth in solder interconnects, Physica A 468 (2017) 195–204, https://doi.org/10.1016/j.physa.2016.11.016.
[52] Y. Wang, Y. Yao, A theoretical analysis of the electromigration-induced void morphological evolution under high current density, Acta Mech. Sin. 33 (2017) 868–878, https://doi.org/10.1007/s10409-017-0645-z.
[53] Y. Yao, Y. Wang, L.M. Keer, M.E. Fine, An analytical method to predict electromigration-induced finger-shaped void growth in SnAgCu solder interconnect, Scr. Mater. 95 (2015) 7–10, https://doi.org/10.1016/j.scriptamat.2014.08.028.
[54] Y. Li, J.S. Moor, B. Pathangey, R.C. Dias, D. Goyal, Lead-free solder joint void evolution during multiple subsequent high-temperature reflow, IEEE Trans. Device Mater. Reliab. 12 (2012), https://doi.org/10.1109/TDMR.2012.2190736.
[55] L. Qu, H.T. Ma, H.J. Zhao, A. Kunwar, N. Zhao, In situ study on growth behavior of interfacial bubbled and its effect on interfacial reaction during a soldering process, Appl. Surf. Sci. 305 (2014) 133–138, https://doi.org/10.1016/j.apsusc.2014.03.003.
[56] O. Kraft, E. Artz, Electromigration mechanisms in conductor lines: void shape changes and slit-like failure, Acta Mater. 45 (1997) 1599–1611, 1359-6454/97.
[57] B. Sun, Z. Suo, W. Yang, A finite element method for simulating interface motion – I. Migration of phase and grain boundaries, Acta Mater. 45 (1997) 1907–1915, 1359-6454/97.
[58] J.M. Blakely, Introduction to the Properties of Crystal Surfaces, Pergamon Press, 1973.
[59] H.X. Qian, W. Zhou, Y.Q. Fu, B.K.A. Ngoi, G.C. Lim, Crystallographically-dependent ripple formation on Sn surface irradiated with focused ion beam, Appl. Surf. Sci. 240 (2005) 140–145, https://doi.org/10.1016/j.apsusc.2004.06.101.
[60] M.S. Sellers, A.J. Schultz, C. Bararan, D.A. Kofke, Atomistic modeling of β-sn surface energies and adatom diffusivity, Appl. Surf. Sci. 256 (2010) 4402–4407, https://doi.org/10.1016/j.apsusc.2012.02.038.
[61] P. Eckhold, M.S. Sellers, R. Niewa, W. Hugel, The surface energies of β-Sn — a new concept for corrosion and whisker mitigation, Microelectron. Reliab. 55 (2015) 2799–2807, https://doi.org/10.1016/j.microrel.2015.08.018.
[62] D.J. Pete, J.B. Helonde, A.V. Vairagar, S.G. Mhaisalkar, A model for understanding electromigration-induced void evolution in dual-inlaid Cu interconnect structure, J. Electron. Mater. 41 (2012), https://doi.org/10.1007/s11664-011-1855-y, 586-572.
[63] T.O. Orgutani, E.E. Oren, Electromigration-induced void grain-boundary interactions: the mean time to failure for copper interconnects with bamboo and near-bamboo structures, J. Appl. Phys. 96 (2004) 7246, https://doi.org/10.1063/1.1815389.
[64] Y.C. Hu, Y.H. Lin, C.R. Kao, K.N. Tu, Electromigration failure in flip chip solder joints due to rapid dissolution of copper, J. Mater. Res. 18 (2003), https://doi.org/10.1557/JMR.2003.0355.
[65] S.J. Subramanian, P. Sofronis, P. Ponte Castaneda, Void growth in power-law creeping solids: effect of surface diffusion and surface energy, Int. J. Solids Struct. 42 (2005) 6202–6225, https://doi.org/10.1016/j.ijsolstr.2005.06.048.
[66] S. Belyakov, H.V. Atkinson, S.P.A. Gill, Crystallographically faceted void formation in the matrix of lead-free solder joints, J. Electron. Mater. 39 (2010), https://doi.org/10.1007/s11664-010-1184-6.